J. Fluid Mech. (2005), *vol.* 526, *pp.* 117–146.
DOI: 10.1017/S0022112004002721 Printed in the United Kingdom

On low-frequency modulations and three-dimensionality in vortex shedding behind a normal plate

By S. J. WU[1], J. J. MIAU[1]†, C. C. HU[1] AND J. H. CHOU[2]

[1]Department of Aeronautics and Astronautics, National Cheng-Kung University, Tainan, Taiwan 70101

[2]Department of Engineering Science, National Cheng-Kung University, Tainan, Taiwan 70101

(Received 10 December 2003 and in revised form 1 October 2004)

In this study spanwise correlation measurements and smoke flow visualization were performed on vortex shedding behind a normal plate. For Reynolds numbers in a range between 1800 and 27 000, the hot-wire signals measured were analysed by a wavelet transformation, from which the instantaneous properties of vortex shedding were obtained and examined. Results show that the phase difference of vortex shedding detected at two spanwise locations, separated by twice the characteristic length, can be as high as 35°. A correlation analysis further shows that large spanwise phase differences occur when small fluctuating amplitudes in the vortex shedding signals are measured. Smoke-wire visualization performed at Reynolds number 1800 indicates that the formation of shedding vortex can be divided into two distinct situations, namely, one featuring a long formation region, called Mode L; and the other featuring a short formation region, called Mode S. In Mode S, the three-dimensionality of vortex formation appears to be very pronounced, and the secondary vortices are clearly present in the separated shear layer. The events of Mode S occupy less than 5% of the total time measured, and are called the burst events in this study.

1. Introduction

Some early observations concerning the low-frequency behaviour of vortex shedding behind a bluff body can be found in Roshko (1954), Tritton (1959), Bloor (1964), Gerrard (1967) and Hanson & Richardson (1968). Since then, this flow behaviour has attracted quite a number of studies. The low-frequency variations measured in the vortex shedding signals were often attributed to the three-dimensionality of flow. Studies on the three-dimensional characteristics of vortex shedding behind a two-dimensional bluff body can be traced to the early work by Grant (1958). The flow visualization results provided by Wei & Smith (1986), Cimbala, Nagib & Roshko (1998), Williamson (1988), Bays-Muchmore & Ahmed (1993) and Wu *et al.* (1994) clearly showed the presence of streamwise vortices, called the secondary vortices, in the near-wake region behind a circular cylinder. The secondary vortices were recognized as an important feature of the three-dimensionality of vortex shedding.

Roshko (1993) attributed the three-dimensionality of wake flows to extrinsic and intrinsic effects. One of the extrinsic effects is the aspect ratio of a bluff body (Graham 1969; Fox & West 1990; Szepessy & Bearman 1992; Norberg 1994). Discussions on

† Author to whom correspondence should be addressed: jjmiau@mail.ncku.edu.tw

the arrangement of end plates can be found in Stansby (1974), Gerich & Eckelmann (1982) and Stäger & Eckelmann (1991). The extrinsic effect can also be due to the structural characteristics of the bluff body (Gaster 1969; Van Atta & Gharib 1987; Lewis & Gharib 1992; Bearman & Tombazis 1993). Low-frequency modulations in vortex shedding were noted in studies with axisymmetric models, for instance a sphere by Taneda (1978), a circular disk by Berger, Scholz & Schumm (1990), and an elliptic disk by Kiya & Abe (1999). On the other hand, the intrinsic characteristics of three-dimensionality are seen in the experimental results of Williamson (1992, 1996), Yang, Mansy & Williams (1993) and Blackburn & Melbourne (1996), and the numerical results of Henderson (1997) and Najjar & Balachandar (1998). Lisoski (1993) further showed that in reality both the intrinsic and extrinsic effects can be present in a wake flow.

In the previous studies on low-frequency modulations embedded in the vortex shedding process, the instantaneous behaviour of vortex shedding was also of interest. Gerrard (1966) found that in the stable range of vortex shedding (Reynolds number $Re = 85$), the modulations in the hot-wire signals measured downstream of a circular cylinder were directly related to the differences of the vortex shedding frequencies measured at different time instants, and also to the flapping of the wake. In the transition range ($Re = 235$), the relation found at $Re = 85$, that the maximum amplitude in the signals measured was coupled with the minimum period of vortex shedding, was approximately correct. In the turbulent range ($Re = 20\,000$), no evidence is available concerning the flapping of the wake, or the correlation between modulations of the signal amplitude and the shedding periods. Analysing the signals measured by flush-mounted thermal films on a circular cylinder at Reynolds numbers from 20 000 to 40 000, Blevins (1985) pointed out that the vortex shedding process was a series of coherent strings of events whose frequencies wandered by 1%–2% about the nominal vortex shedding frequency. He noticed a tendency that the larger the amplitude, the lower the vortex shedding frequency. Norberg (1989) presented a probability density distribution of the vortex-shedding frequencies obtained from his measurements. He noted that the signal bursts featuring larger fluctuating amplitudes were associated with shedding frequencies lower than the mean value. Unfortunately, the reports mentioned above were not able to resolve the vortex shedding frequency to a local time, thus the variations of vortex shedding frequency could not be described in a quantitative manner.

Recently, the present authors (Miau *et al.* 2004) have made an attempt, employing a wavelet transformation, to obtain the vortex shedding frequency from the hot-wire signals measured in the near-wake region behind a normal plate. This analysis showed that the instantaneous vortex shedding frequencies obtained were in good correlation with the low-frequency modulations in the signals. This finding lends support to an earlier observation that the low-frequency modulations in vortex shedding are linked closely with the unsteady variations of the vortex formation length in the near-wake region (Miau *et al.* 1999). To explore the link between low-frequency modulations and three-dimensionality in vortex shedding, Miau *et al.* (2003) detected the spanwise motions of flow in a separated shear layer using a split-fibre probe. The characteristics of the low-frequency component embedded in the spanwise motions were found to be similar to those in the streamwise velocity fluctuations measured by a normal hot wire.

Based on the previous findings (Miau *et al.* 2003, 2004), the present work is aimed at examining the vortex shedding characteristics at different spanwise locations, in order to gain a better understanding of the unsteady, three-dimensional behaviour of flow

in the near-wake region. Of particular interest are the instantaneous characteristics of vortex shedding along the spanwise direction, based on the quantities obtained by a wavelet analysis.

2. Experimental methods

A closed-return low-speed wind tunnel was employed for the present study. The test section was 150 mm by 150 mm in cross-section. A pitot tube was mounted at the entrance of the test section to monitor the free-stream velocity, called U_0. Turbulence intensity measured at the centreline of the test section was about 0.7% of U_0, for U_0 between 2 and 20 ms^{-1}. Efforts were made to confirm that no extraneous fluctuating components were present in the free-stream flow. The non-uniformity of the mean flow distribution in the test section, excluding the boundary-layer regions along the walls, was verified to be within $\pm 0.5\%$.

Referring to figure 1, a normal plate of trapezoidal cross-section was employed as the bluff body for the present study. Its maximum width facing the incoming flow was 32 mm, denoted as D. Based on D, the geometrical blockage ratio due to the bluff plate spanning between the sidewalls of the test section is about 21%, and the aspect ratio of the normal plate is 4.7. The Reynolds number, Re, based on D and U_0, was fixed at 1.8×10^3 for the smoke-wire flow visualization experiment, and varied in a range between 1.8×10^3 and 2.7×10^4 during the hot-wire velocity measurements. It is noted that the present bluff configuration of high blockage and low aspect ratio is not ideal as a two-dimensional model for experiments. As the geometrical characteristics of the bluff body could influence the three-dimensionality of vortex shedding structures (Roshko 1993; Norberg 1994), care should be taken when applying the present results to other flow configurations. In view of this, the differences in the characteristics of low-frequency modulations and three-dimensionality of vortex shedding seen in the present flow and other wake flow configurations would be of interest.

Figure 1 presents a cross-sectional view of the normal plate at the mid-span, and the coordinate system employed for the present study is indicated. X denotes the streamwise axis pointing downstream, with $X = 0$ at 6.5 mm downstream of the frontal face of the normal plate. Y denotes the vertical axis, with $Y = 0$ located at the centreline of the test section. Z denotes the spanwise axis, with $Z = 0$ located at the mid-span of the model.

In this study, single normal hot-wire probes, Dantec 55P11, were employed to sense the velocity fluctuations in the free stream. In addition, a smoke-wire flow visualization technique was employed to obtain the images of flow in the near-wake region, with a smoke wire orientated in the Y- or Z-direction upstream of the bluff plate. Hence, a top or side view of the separated shear layer originated from the normal plate could be examined.

3. Wavelet analysis

Wavelet transformation (WT) was employed in this study to obtain instantaneous information on vortex shedding from the raw hot-wire signals. The principle of WT is briefly described below. WT of a signal trace $g(t)$ with respect to a wavelet function $\psi(t)$ is defined by a convolution integral (Grossman & Morlet 1984):

$$W(a, b) = \frac{1}{\sqrt{a}} \int g(t) \psi^* \left(\frac{t - b}{a} \right) \mathrm{d}t, \tag{1}$$

(*a*)

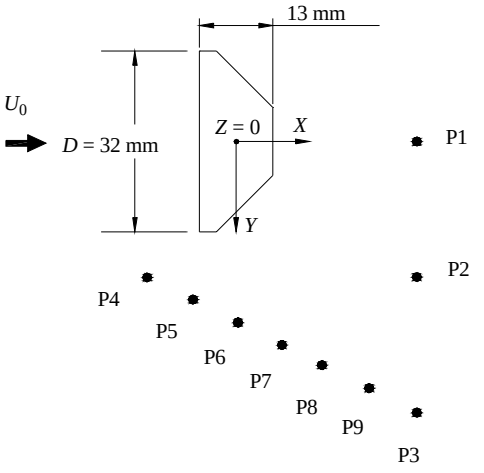

	X/D	*Y/D*	*Z/D*
P1	1	0	0
P2	1	0.75	0
P3	1	1.5	0
P4	–0.5	0.75	0
P5	–0.25	0.875	0
P6	0	1	0
P7	0.25	1.125	0
P8	0.5	1.25	0
P9	0.75	1.375	0

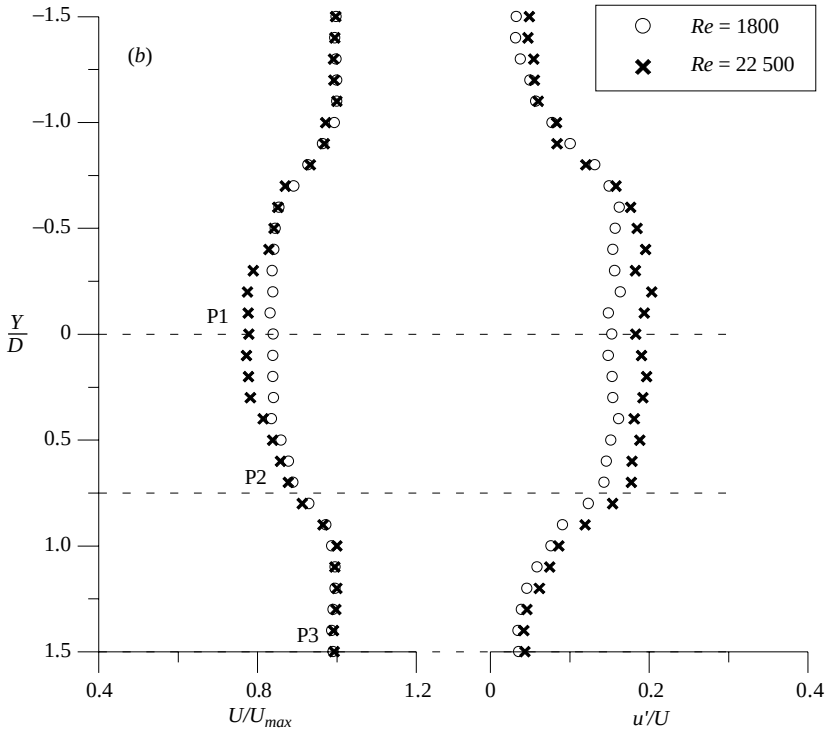

FIGURE 1. (*a*) Schematics of the cross-sectional view of the normal plate at $Z/D = 0$, the coordinate system employed, and the locations of the hot wire S2. (*b*) The mean velocity and velocity fluctuation intensity profiles obtained at $X/D = 1$ by a normal hot wire, in which U and u' denotes the local mean velocity and root-mean-square velocity fluctuation, respectively, and U_{max} denotes the maximum value in the corresponding velocity profile.

where a denotes the scale, b denotes the translation, and ψ^* is the complex conjugate of ψ. For ψ in (1), a continuous Morlet wavelet in the following form was adopted:

$$\psi(T) = \exp(\mathrm{i}k_\psi T)\exp(-T^2/2), \tag{2}$$

where the parameter k_ψ was taken to be 6.0 to satisfy the admissibility condition (Farge 1992). The selection of this Morlet wavelet was based on the following considerations: (*a*) to yield the most detailed multi-scale structure of the velocity fluctuations (Ishikawa *et al.* 1996), and (*b*) to give a satisfactory performance for the present signals measured (Hamdan *et al.* 1996). After the wavelet function, ψ, and the associated parameters had been determined, the computation according to (1) could be carried out.

The wavelet coefficient $W(a, b)$ in (1) can be analytically transformed into $W(f, t)$ (Torrence & Compo 1998), where f and t are the frequency and time, respectively, associated with the signals analysed. Thus, the wavelet analysis is capable of providing information on a frequency component at a given time instant of the signals analysed.

For the present purpose, the vortex-shedding frequency at a given time instant and its amplitude and phase are obtainable by WT. Referring to Carmona, Hwang & Torrésani (1997), the vortex shedding frequency can be determined as the peak among all the moduli of the wavelet coefficients. This process is further explained below.

(*a*) Find f_{max} at a time instant, t, for which the modulus $|W(f_{max}, t)|$ is the maximum among all the moduli of the frequency components obtained.

(*b*) Apply (*a*) to all the sampled time instants, and combine $\{f_{max}, t\}$ pairs to compose the vortex shedding frequency $f_w(t)$ as a function of t.

The modulus associated with $f_w(t)$ is denoted as $A_w(t)$, and called the amplitude of the vortex shedding frequency:

$$A_w(t) = |W(f_{max}(t), t)|. \tag{3}$$

For any frequency f at a given instant t, its phase $\theta(f, t)$ can be further defined as

$$\theta(f, t) = \tan^{-1}\frac{\mathrm{Re}(W(f, t))}{\mathrm{Im}(W(f, t))}, \tag{4}$$

where Re and Im denote the real and imaginary parts of $W(f, t)$, respectively. Consequently, following (4) a phase function corresponding to $f_w(t)$, called $\theta(f_w, t)$, can be defined. Similarly, a phase function corresponding to the frequency f_s, denoting the time-mean vortex-shedding frequency, can also be defined, called $\theta(f_s, t)$.

Figure 2(*a*) presents the phase functions $\theta(f_w, t)$ and $\theta(f_s, t)$ obtained from a segment of the raw signals obtained at $Re = 1800$. Figure 2(*b*) indicates the difference between these two functions, which appears to be limited to a range of $\pm 3^\circ$. These differences are rather small compared to the spanwise phase variations which will be shown later. The phase information obtained will be of use later to examine the phase difference of vortex shedding at different spanwise locations, an indication of the degree of three-dimensionality of the flow. In the following, the phase function $\theta(f_w, t)$ will be used for analysis.

Table 1 lists the parameters of the present wavelet transformation for all the Reynolds numbers studied. As seen, the sampling rate and time length of the hot-wire data taken were varied with the Reynolds number. The frequency resolution in the neighbourhood of f_s was varied with the Reynolds number as well. For the hot-wire measurements at a point, usually 30 sets of data were gathered, from which an uncertainty analysis could be carried out along with the mean value reduced (Bendat & Piersol 1991).

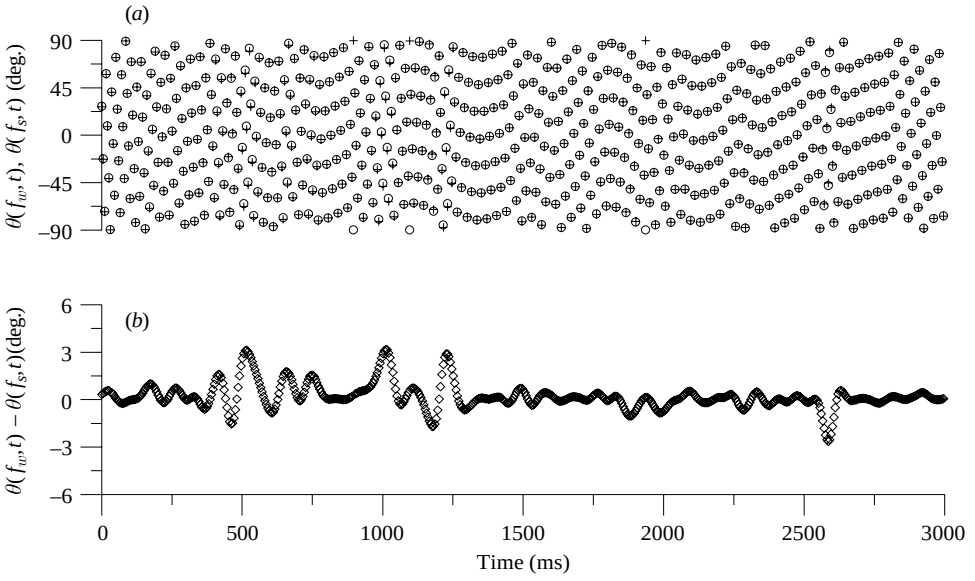

FIGURE 2. (*a*) $\theta(f_w, t)$ (○) and $\theta(f_s, t)$ (+) obtained at $Re = 1800$; (*b*) the difference between $\theta(f_w, t)$ and $\theta(f_s, t)$.

Reynolds number	Sampling rate (s^{-1})	Sampling time (s)	f_s (Hz)	Frequency resolution of WT at f_s(Hz)
1800	200	20	6.0	0.029
4100	200	20	12.1	0.060
5200	250	16	15.1	0.061
7700	500	8	22.0	0.044
9800	500	8	28.8	0.057
16 000	1000	4	45.4	0.045
22 500	1000	4	63.5	0.064
27 000	1000	4	75.4	0.075

TABLE 1. Parameters of wavelet transformation in the present study.

4. Results and discussion

4.1. *Results of smoke-wire visualization*

Figures 3(*a*) and 3(*b*) present two sets of smoke-wire visualization images obtained from the top-view of the separated shear layer originating from the normal plate, for a spanwise region of $Z = \pm D$. The two sets of images were taken with reference to two arbitrary instants t_a and t_b, respectively. The time instant corresponding to each of the images taken is indicated in the upper right corner. Note that the images shown in figure 3(*a*) span a time length of about $2T_s$, where T_s denotes the mean vortex shedding period. In general, these images reveal the unevenness of roll-up of the separated shear layer along the spanwise direction. As a rough estimate from the appearances of the smoke streaks, the spanwise variations can be as large as $0.5D$, or up to 30° inclination with respect to the spanwise axis. Gerrard (1966) obtained the inclination angle of the vortex lines from oscillograms, and found that the inclinations varied within ±15° about the spanwise axis. In addition, Gerrard (1966) conducted a

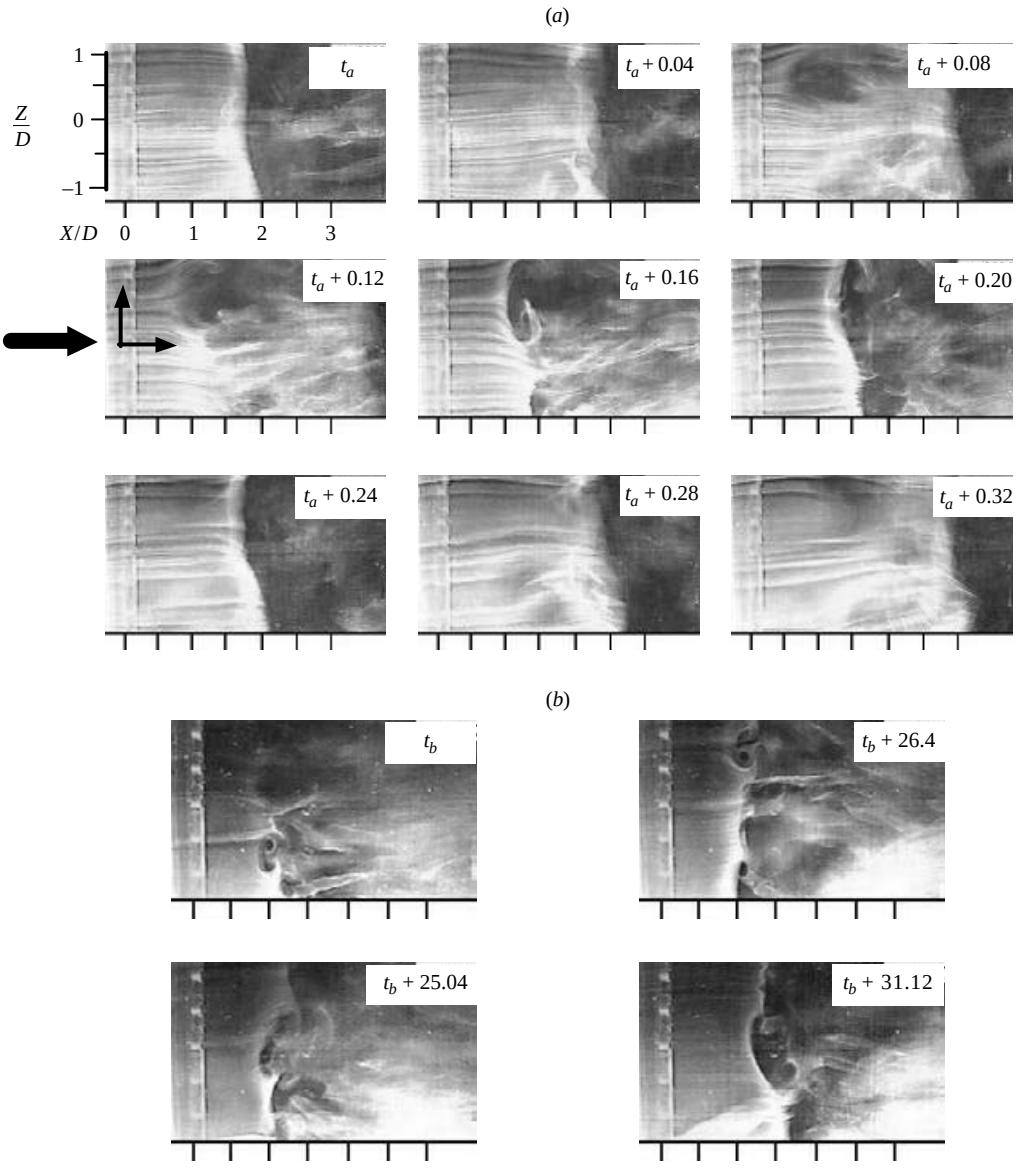

FIGURE 3(a, b). For caption see next page.

review of the inclined angles of the vortex lines reported in the literature, and found that they fall in a range between 5° and 30°.

Another striking phenomenon revealed in figure 3(a, b) is that at some instants secondary vortices, mostly in the form of horse-shoe vortices, developed in the separated shear layer. In particular, the images in figure 3(b) highlight the presence of mushroom-shaped structures in the streamwise region of $X/D = 1$ to 1.5. These look very similar to the secondary streamwise eddies reported by Wei & Smith (1986), who conducted the hydrogen bubble visualization experiments at Reynolds numbers ranging from 1000 to 4350. Also, Wu *et al.* (1994) conducted flow visualization experiments at Reynolds numbers between 50 and 1800, and pointed out that the formation of streamwise vortices is the main feature of the three-dimensional structure

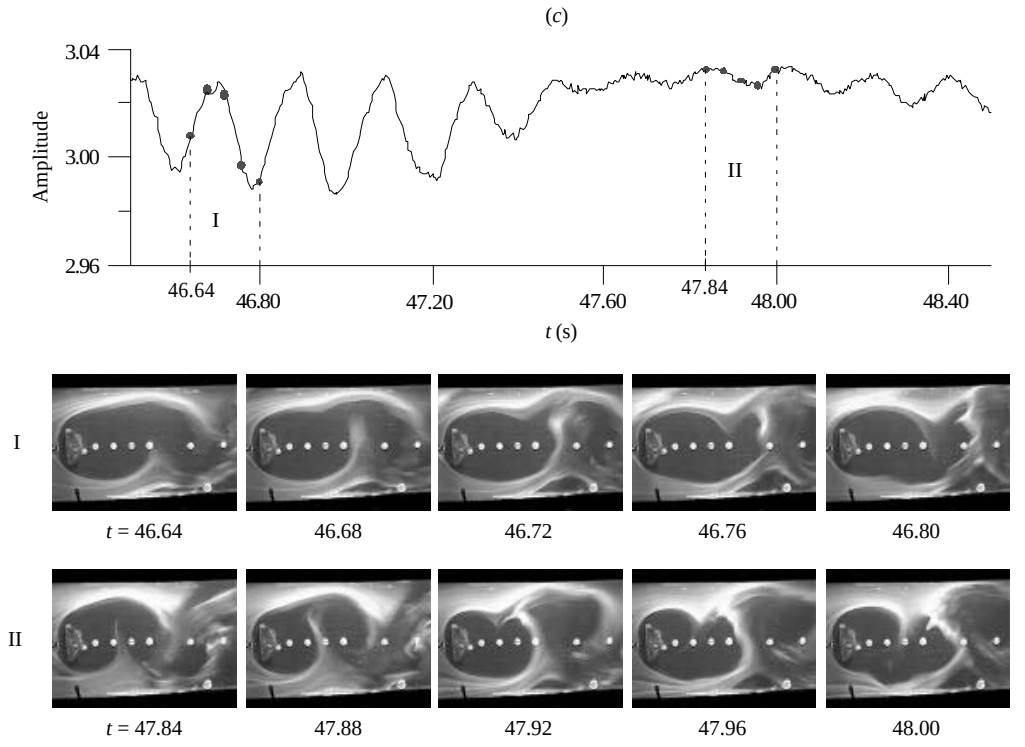

FIGURE 3. Smoke-wire visualization obtained at $Re = 1800$, for $T_s = 0.167$ s. (*a*) Spanwise variations of the streamwise extent of the vortex formation region within two vortex shedding periods; (*b*) evidence of secondary vortices in the separated shear layer; (*c*) the smoke streakline patterns obtained in an X, Y plane near $Z = 0$, during the time periods I and II indicated in the hot-wire signals above, which were obtained at $(X/D, Y/D, Z/D) = (1, 1.5, 0)$. (*c*) Reproduced from Miau *et al.* (2004). (Time unit: second.)

of the wake behind the bluff cylinder. The images in figure 3(*b*) indicate that the secondary vortices developed in the separated shear layer occur randomly in space and are inclined at various angles with respect to the spanwise axis. From these images, a rough estimate of the length scale of a pair of secondary vortices gives the value of D, and the cross-sectional size of a secondary vortex ranges between $0.2D$ and $0.5D$.

Concerning the characteristic size of the secondary vortices in the separated shear layer associated with vortex formation, table 2 contains a survey of the previous findings. Interestingly, these findings consistently indicate that the size is comparable to the characteristic length of the bluff body.

The images in figure 3(*c*) show the unsteady appearance of the separated shear layer in the near-wake region from a side view, which are reproduced from Miau *et al.* (2004). An interesting feature revealed is that the size of the vortex formation region is varying with time, seen from a comparison of the images corresponding to the time periods I and II. The vortex formation region here refers to the maximum extent to which a separation vortex can grow before shedding. This statement is somewhat different from that normally given in the literature, which is the extent of vortex formation in the time-mean sense (Szepessy & Bearman 1992; Miau *et al.* 1999). With the smoke-wire visualization images shown, the size of the vortex formation region can be estimated qualitatively. Within period I, the streamwise extent of the vortex formation region is estimated to be slightly larger than $2D$. Note that in each

Source	Reynolds number	Method	Scale of spanwise structure	Spanwise phase difference
Humphreys (1966)	$40 \sim 600 \times 10^3$	Silk threads visualization	$1.4D \sim 1.7D$	
Toebes (1969)	68×10^3	Hot wires		Max. value of 120° at $2.5D$
Blevins (1985)	40×10^3	Flush film & hot film		Max. value of 180° at $6D$
Williamson (1988)	200 (mode A)	Flow visualization	$3D$ (spanwise wavelength)	
	> 240 (mode B)		D (spanwise wavelength)	
Szepessy & Bearman (1992)	57×10^3	Pressure tap & hot wire	$2.5D$ (correlation length)	Max. value of 180° at $2.5D$
Bays-Muchmore & Ahmed (1993)	$330 \sim 21 \times 10^3$	Hydrogen bubble visualization	D	
Noack *et al.* (1993)	230	Numerical	$1.8D$	
Mansy *et al.* (1994)	$170 \sim 2.2 \times 10^3$	Laser anemometer	$D \sim 1.3D$	
Szepessy (1994)	43×10^3	Pressure taps	up to $2D$ (width of disturbed cell)	Fit by a third-order polynomial in the range $0.25 < \Delta Z/D < 9$, asymptotic value is 104°.
Wu *et al.* (1994)	200	Hydrogen bubble	$0.90 \sim 0.95D$ (spanwise wavelength)	
	$1000 \sim 1800$		$0.70 \sim 0.80D$ (spanwise wavelength)	

TABLE 2. A survey of studies on the spanwise scale of secondary vortices and the spanwise phase difference of shedding vortices.

of the images, the spacing between two neighbouring white dots in the near-wake region is $0.5D$. On the other hand, within period II the streamwise extent of the vortex formation region is estimated to be about $1D$–$1.5D$. Referring to the raw hot-wire signals, included for reference, one sees that the fluctuating amplitude of the velocity signals within period I appears to be substantially larger than that within period II. For a quantitative investigation of the relation between the instantaneous characteristics of the velocity signals and the unsteadiness of the vortex formation region, refer to Miau *et al.* (2004).

4.2. *Time-mean spanwise correlation*

For spanwise correlation measurements, three normal hot wires, S1, S2 and S3, were aligned in the spanwise direction, evenly separated distance D apart. The hot wire S2 was always situated in the plane of $Z/D = 0$, at one of the points indicated in figure 1, whereas S1 and S3 were situated in the regions $Z/D < 0$ and $Z/D > 0$, respectively. Thus, the spanwise separation, ΔZ, of any two of the three hot wires can be either D or $2D$. These spanwise separations were chosen to match the length scale of the secondary vortices, found from the preceding smoke flow visualization and table 2.

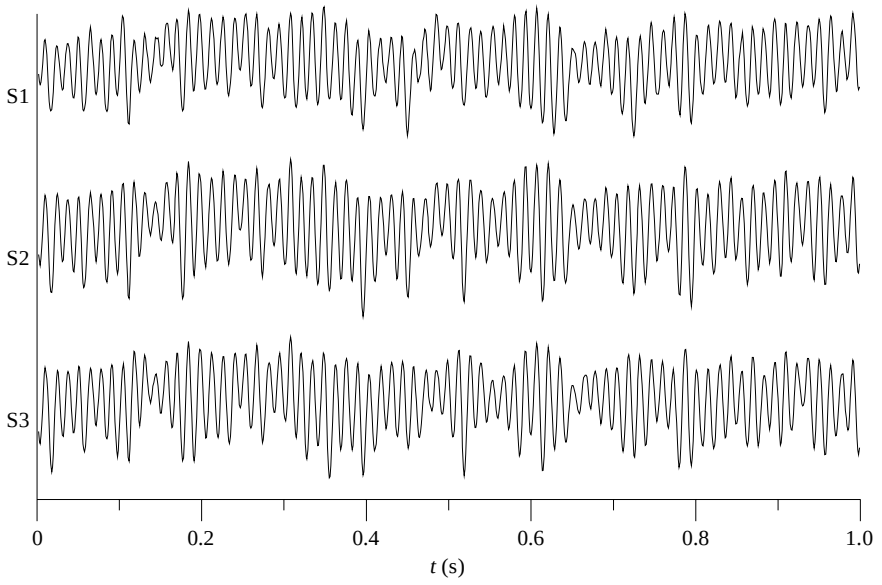

FIGURE 4. Sampled signals of the hot wires S1, S2 and S3, with S2 at $(X/D, Y/D, Z/D) = (0.5, 1.25, 0)$, and $Re = 27\,000$.

Velocity measurements were mainly performed outside the wake shear layer. Referring to figure 1, the locations P3–P9, in the plane of $Z = 0$, indicate where the velocity measurements were performed and will be reported later in the paper. Also included in the figure are the streamwise velocity and velocity-fluctuation intensity profiles obtained at $X/D = 1$, revealing that the point P3 is located in the free stream, whereas the point P2 is located at the edge of the separated shear layer. As these velocity measurements were made with a normal hot-wire probe, the data in the neighbourhood of the point P1 should be considered for qualitative reference only, since reversed flow could possibly take place.

Figure 4 presents the sampled signal traces of the three hot wires, with S2 located at $(X/D, Y/D, Z/D) = (0.5, 1.25, 0)$. A quick glance easily identifies low-frequency amplitude modulations in all the three signal traces, and appear to be in phase, roughly speaking. Thus, one can say that low-frequency modulations existing in the near-wake region are of global nature (Miau *et al.* 1999).

A close look at figure 4, reveals that the amplitude and phase of velocity fluctuations at three spanwise locations do not perfectly coincide. These differences can be further revealed by a correlation analysis. Figure 5 shows the cross-correlation coefficients of the hot-wire traces S1 and S2 (abbreviated as S1–S2), and S1 and S3 (abbreviated as S1–S3), at zero time lag, for Re between 1800 and 27 000. The solid symbols in figure 5 denote the cross-correlation coefficients of S1–S2, where ΔZ was D, and the open symbols corresponding to the correlation coefficients of S1–S3, where ΔZ was $2D$. Since the hot wires were located outside the shear layer, the velocity fluctuations measured are essentially due to the potential fluctuations associated with vortex shedding. At $Re = 1800$, the correlation coefficient values of S1–S2 and S1–S3 are 0.93 and 0.85, respectively, signifying that the spanwise coherence of vortex shedding structures is very pronounced. At $Re = 27\,000$, the values of S1–S2 and S1–S3 are reduced somewhat, i.e. to 0.82 and 0.74, respectively. In the range of Reynolds numbers studied, the cross-correlation coefficients obtained decrease as the

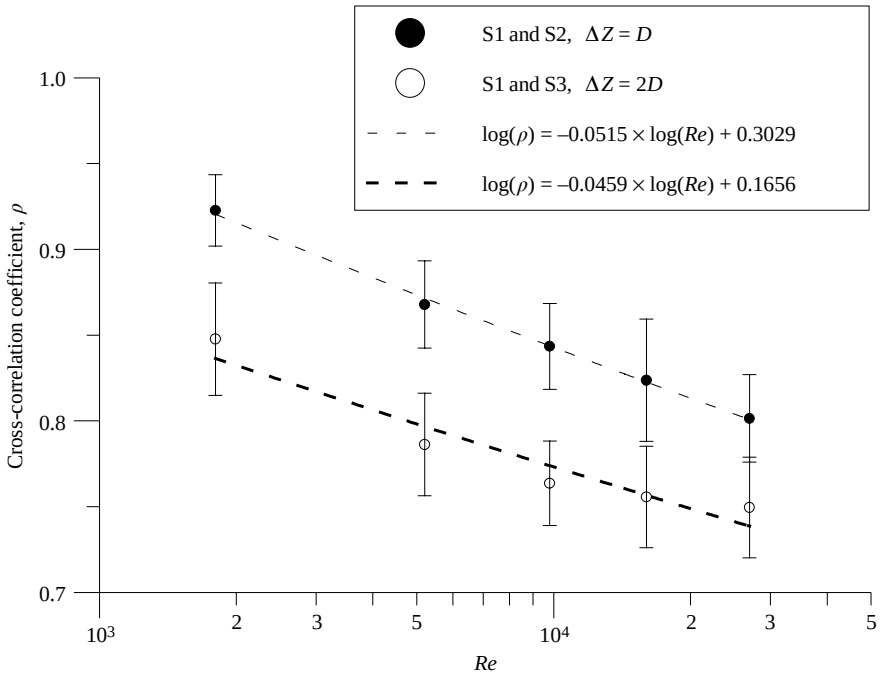

FIGURE 5. Correlation coefficients between the hot-wire signals S1–S2 and S1–S3, with S2 at $(X/D, Y/D, Z/D) = (0.5, 1.25, 0)$, for $Re = 1800$ to 27 000.

Reynolds numbers increase. The trend can be fitted by the dashed lines in figure 5, which implies that the three-dimensionality of the flow becomes more pronounced as the Reynolds number increases. The same statement was made by Wang (2000), concluded from dye visualization of the wake flow behind a normal plate in a water channel, for Reynolds numbers in a range of 1220 to 5670.

The correlation coefficients shown in figure 5 are higher than the values reported by Toebes (1969) and Szepessy (1994), whose experiments were performed with circular cylinders. Szepessy (1994) showed that the spanwise correlation coefficients of pressure measurements made at the circumferential angle 90° of a circular cylinder were about 0.8 and 0.6 for $\Delta Z = D$ and $2D$, respectively. Toebes (1969) reported smaller values of 0.7 and 0.5, according to hot-wire measurements made in a wake flow. The discrepancies between the coefficient values obtained in the present study and given by these two references could be due to a number of factors, including Reynolds number, geometry and aspect ratio of the bluff cylinder, and the flow quantities measured. Further discussion on these factors is beyond the present scope. On the other hand, a common feature revealed from the results of these studies is that a significant reduction in the correlation values is noted when the spanwise separation is increased from D to $2D$. This could be attributed to the formation of shedding vortices slanted with respect to the spanwise axis, in which the secondary vortices could develop. Given the fact that the secondary vortices take place randomly in space and unsteadily in time in the near-wake region, the level of correlation between two signals would drop considerably due to the increase of spanwise separation. (Szepessy 1994) The increasing of the spanwise separation from D to $2D$ certainly promotes the possibility of the presence of secondary vortices.

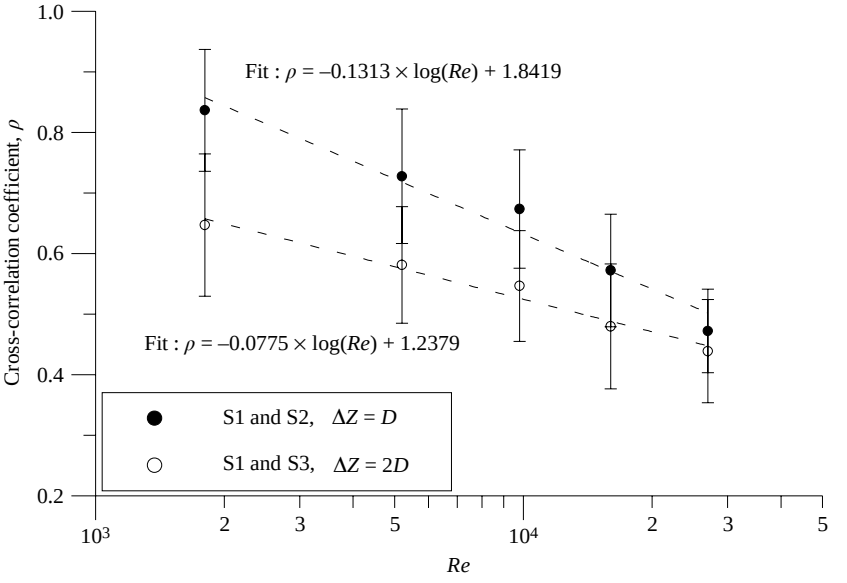

FIGURE 6. Correlation coefficients of $A_w(t)$ of the hot-wire signals S1–S2, and S1–S3, for S2 at $(X/D, Y/D, Z/D) = (0.5, 1.25, 0)$, and $Re = 1800$ to 27 000.

4.3. *Correlation between low-frequency modulations and instantaneous vortex shedding frequency*

The results of the present wavelet analysis of the measured hot-wire signals give the desired values of the vortex shedding frequency, $f_w(t)$, and the associated amplitude, $A_w(t)$. In the following, $f_w(t)$ and $A_w(t)$ obtained at different spanwise locations will be examined with a correlation analysis. First of all, figure 6 presents the spanwise correlation coefficients of $A_w(t)$ of S1–S2, and S1–S3, with S2 located at $(X/D, Y/D, Z/D) = (0.5, 1.25, 0)$, for the Reynolds numbers studied. Similarly to figure 5, the correlation values of $\Delta Z = D$ appear to be higher than those of $\Delta Z = 2D$, and decrease as Re increases. Compared to figure 5, the data in figure 6 indicate that the correlation coefficients are lower in value, and decay with Reynolds number in a more pronounced manner.

Essentially, figure 5 shows the spanwise correlation of total velocity fluctuations, including the components of vortex shedding frequency and low-frequency modulations; whereas figure 6 concerns specifically the spanwise correlation of the latter component. This statement is based on an observation that the quantity $A_w(t)$ can represent well the low-frequency modulations in the signals measured. For this, one may also refer to figure 13 below for a comparison of the raw signals and the corresponding $A_w(t)$ curve.

A remark on the spanwise correlation of the low-frequency modulations is made below. Referring to Miau *et al.* (2003), the spanwise correlation of the low-passed base pressure signals obtained with the same bluff body, at $Re = 16\,000$, gave the coefficient values of 0.38 to 0.34 for $\Delta Z = 0.5D$ to $1.5D$. In figure 6, the correlation coefficients of S1–S2 and S1–S3 obtained at $Re = 16\,000$ are 0.57 and 0.48, respectively, which are considerably higher than those in Miau *et al.* (2003). This is attributed to the observation that the base pressure signals reported in Miau *et al.* (2003), even low-passed, contained more randomly fluctuating components than those of the present hot-wire signals obtained in the free stream. As a result, the low-frequency

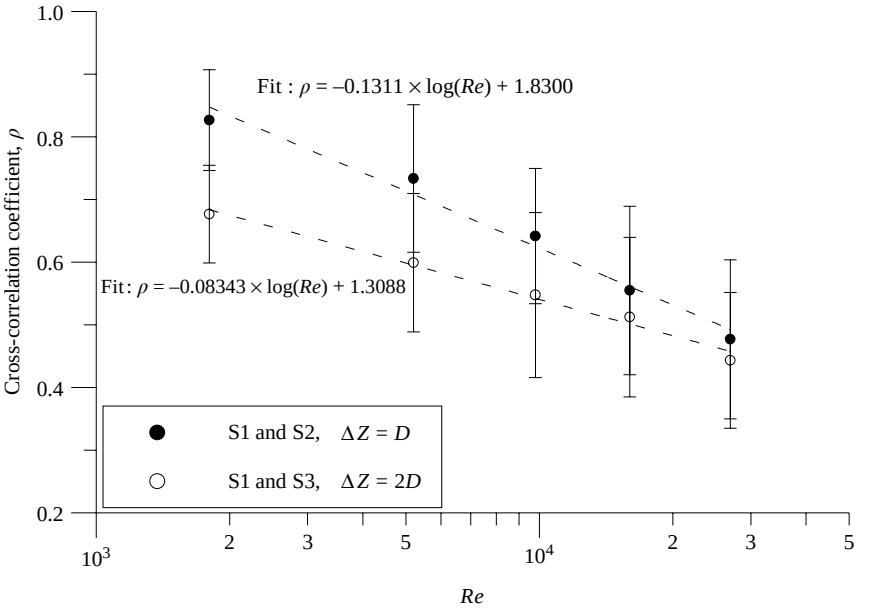

FIGURE 7. Correlation coefficients of $f_w(t)$ of the hot-wire signals S1–S2, and S1–S3, for S2 at $(X/D, Y/D, Z/D) = (0.5, 1.25, 0)$, and $Re = 1800$ to 27 000.

modulations detected in the present study show higher spanwise correlation values than those associated with the base pressure fluctuations.

Figure 7 presents two distributions of spanwise correlation of $f_w(t)$ versus the Reynolds numbers studied, for $\Delta Z = D$ and $2D$, respectively. The hot-wire probes were situated at the same locations as in figure 6. The distributions in this figure bear a similarity to those of $A_w(t)$ in figure 6. The correlation results have the implication that the vortex shedding frequencies at different spanwise locations are not identical, although they may stay very similar most of the time. For further details, one may refer to figure 13(*c*) below for a comparison of the $f_w(t)$ curves corresponding to the hot-wire signals S1 and S2.

Besides the spanwise correlation measurements described above, more measurements were carried out with the hot wire S2 at other points indicated in figure 1, and the hot wires S1 and S3 aligned in the spanwise direction. Figure 8 shows the spanwise correlation results of $A_w(t)$ obtained at $Re = 1800$. The most significant correlation is at P5, where the correlation coefficients obtained are about 0.9 and 0.8, for $\Delta Z = D$ and $2D$, respectively. Since the point P5 is located close to the sharp edge of the normal plate, see figure 1, the velocity fluctuations measured are sensitive to the flapping motions of the separated shear layer. Also, in each of the plots in figure 8, the uncertainty interval associated with the mean value at point P5 appears to be the smallest among all the data points shown. Hence, one can say that the spanwise correlation of the low-frequency modulations is very pronounced at the initial development of the separated shear layer. The data in figure 8 consistently show that the level of spanwise correlation of $A_w(t)$ decreases downstream, in a streamwise region of $X/D = -0.25$ to D. This decreasing trend can be fitted by a second-order polynomial, indicated by a dashed line in each of the two plots.

The results of spanwise correlation of $f_w(t)$, not shown here, appear to be very similar to those seen in figure 8 (Wu 2003).

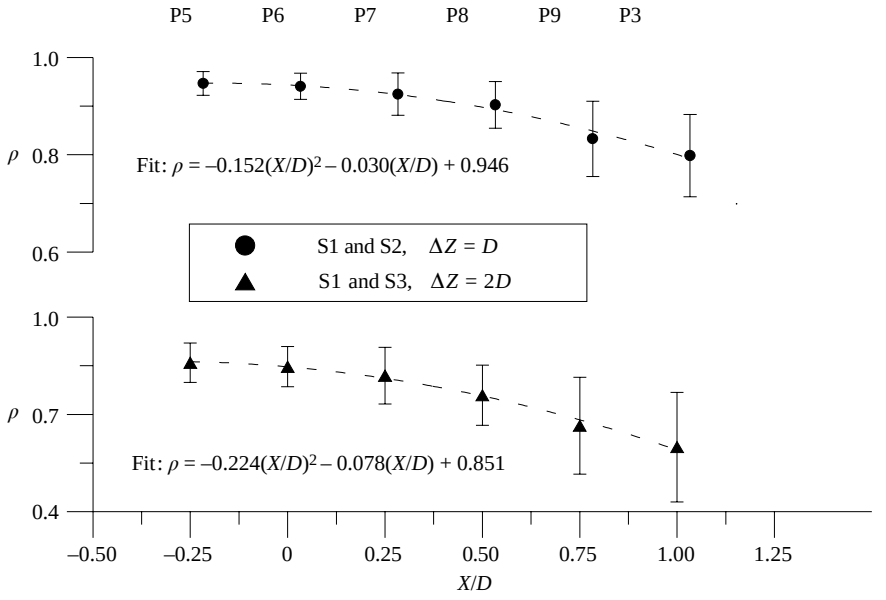

FIGURE 8. Correlation coefficients of $A_w(t)$ of the hot-wire signals S1–S2, and S1–S3, for S2 at the points indicated in figure 1, at $Re = 1800$.

4.4. *Results of instantaneous spanwise phase difference*

According to (4), phase information of the vortex shedding frequency, $\theta(f_w, t)$, can be obtained. Consequently, the phase difference due to vortex shedding at different spanwise locations can be examined. In figure 9, an example illustrating the phase difference between the hot-wire signals S1 and S2 is given. The measurements were made with S2 at $(X/D, Y/D, Z/D) = (1.0, 1.5, 0)$. In figure 9($a$), the sampled hot-wire signals S1 and S2, at $Re = 27\,000$, for a time period of 300 ms, are indicated by the solid and dashed lines, respectively. Figure 9(b) presents the phase functions of $\theta(f_w, t)$ of the hot-wire signals S1 and S2. The phase differences of these two phase functions are shown in figure 9(c). The $\Delta\theta(t)$ values varying with time has the implication that the inclination angles of the shedding vortices vary in time, which reflects the nature of the unsteady, three-dimensional wake flow. The $\Delta\theta(t)$ plot shown also lends support to the unsteady appearance of vortex formation revealed by the smoke flow visualization in figure 3.

The physical relevance of the quantity of $\Delta\theta(t)$ deserves some discussion. The $\theta(t)$ data shown in figure 9(b) are associated with $f_w(t)$ of the hot-wire signals S1 and S2. However, the $f_w(t)$ values obtained at these two points usually do not coincide. Thus, the resultant quantity $\Delta\theta(t)$ in figure 9(c) is somewhat uncertain, physically speaking. Alternatively, one might have considered the spanwise phase differences with reference to a fixed frequency, say f_s. Since the instantaneous vortex shedding frequency is of primary interest here, the definition of $\Delta\theta(t)$ in figure 9 is preferred for analysis. In fact, as pointed out earlier, the differences between the phase functions of $f_w(t)$ and f_s are so small that they can be ignored for the present purpose.

The quantity $\Delta\theta(t)$ can be reduced to the tilting angle of the shedding vortex. The procedures are illustrated below. In figure 9(c), a local maximum $\Delta\theta$ value is found at t about 650 ms. The value read is 19°. With $\Delta Z = D$ and assuming that the

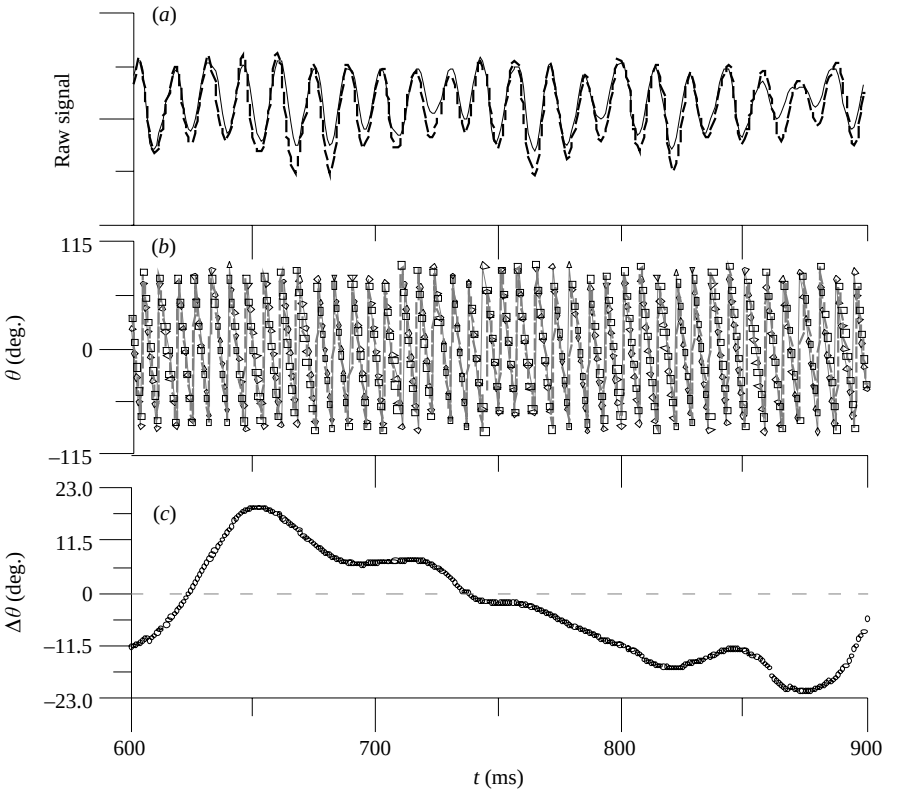

FIGURE 9. (*a*) Sampled hot-wire signals S1 (solid line) and S2 (dashed line), for S2 at $(X/D, Y/D, Z/D) = (1, 1.5, 0)$, and $Re = 27\,000$. (*b*) Phase variations of the instantaneous vortex shedding frequency of the hot-wire signals S1 (square symbols), and S2 (diamond symbols). (*c*) $\Delta\theta(t)$, the phase difference between $\theta(t)$ of S1 and S2.

convection speed of shedding vortices is characterized by U_0,

the characteristic wavelength of shedding vortices: $\dfrac{U_0}{f_s} = \dfrac{D}{St} = \dfrac{D}{0.18} = 5.6D$;

the spanwise tilting of shedding vortex due to 19° phase lag: $5.6D \times \dfrac{19^\circ}{360^\circ} = 0.3D$;

the tilting angle: $\tan^{-1} \dfrac{0.3D}{1D} \cong 16.7^\circ$.

This tilting angle is comparable to the inclination angles of the roll-up of the separated shear layer revealed by the smoke streaks in figures 3(*a*) and 3(*b*), and the findings by Gerrard (1966). To be more specific, the characteristic wavelength of shedding vortices estimated above requires some discussion here. In the near-wake region, the convective speed of shedding vortices would be significantly lower than U_0, and varying along the streamwise direction. Further downstream, the convection speed would probably reach a constant value. In Bloor & Gerrard (1966) and Davies (1976), the convection speed four diameters downstream of a circular cylinder is about $0.8U_0$. Subsequently, assuming that the convection speed of shedding vortices is $0.8U_0$ and following the procedures above, one would obtain a tilting angle 13.5°. Since the shedding vortices could be strongly distorted in the spanwise direction (figure 3), the tilting angles

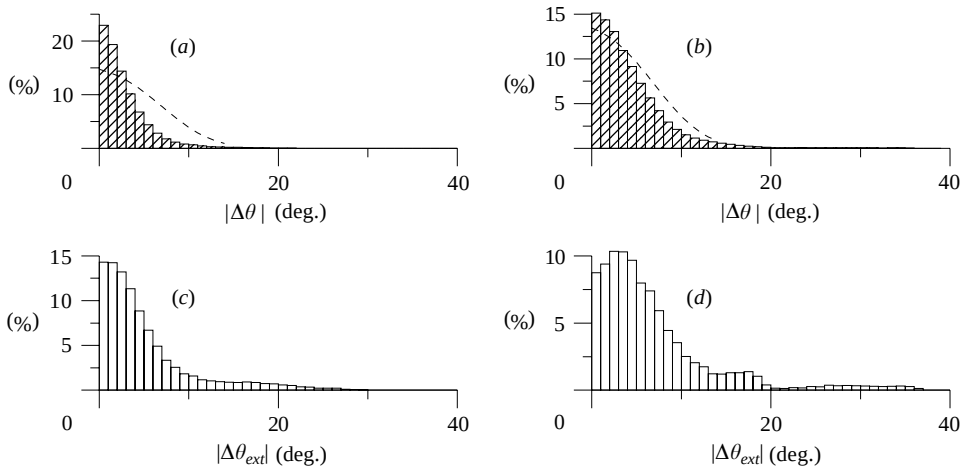

FIGURE 10. Histograms of $|\Delta\theta(t)|$ and $|\Delta\theta_{ext}|$ obtained at $Re = 27\,000$, with S2 at $(X/D, Y/D, Z/D) = (1, 1.5, 0)$: (*a*) $|\Delta\theta(t)|$ of S1–S2; (*b*) $|\Delta\theta(t)|$ of S1–S3; (*c*) $|\Delta\theta_{ext}|$ for $\Delta Z = D$, i.e. $\Delta\theta_{ext}$ samples selected from $\Delta\theta(t)$ of S1–S2 in (*a*); (*d*) $\Delta\theta_{ext}|$ for $\Delta Z = 2D$, i.e. $\Delta\theta_{ext}$ samples selected from $\Delta\theta(t)$ of S1–S3 in (*b*). The dashed lines indicate the Gaussian distribution curves.

mentioned above would merely depict the spatially averaged characteristic over a spanwise distance of D.

In data reduction, it was also verified that the time-averaged value of a $\Delta\theta(t)$ curve was very close to zero. Thus, one can say that the two-dimensional feature of shedding vortices is preserved in the time mean sense.

The statistics of the $\Delta\theta(t)$ values obtained at $Re = 27\,000$, with the hot wire S2 at $(X/D,\ Y/D,\ Z/D) = (1.0, 1.5, 0)$, are presented in the histograms in figure 10. Figures 10(*a*) and 10(*b*) show the histograms corresponding to the $\Delta\theta$ values obtained with $\Delta Z = D$ and $2D$, respectively. Each of the histograms was constructed based on 30 sets of data, each of which contained 4000 sampled points. Note that in these histograms the absolute values of $\Delta\theta$ are presented, since whether there is a phase lead or lag of vortex shedding between the spanwise points examined is not of concern here.

The $|\Delta\theta_{ext}|$ histograms in figures 10(*c*) and 10(*d*) further show the distributions of the local extreme values of $|\Delta\theta(t)|$ in figures 10(*a*) and 10(*b*), respectively. The $|\Delta\theta_{ext}|$ histograms are intended to highlight the statistics of the extreme phase differences. Figure 10(*c*) shows that when $\Delta Z = D$ the $|\Delta\theta_{ext}|$ values can be as high as 29°; and, in figure 10(*d*), when $\Delta Z = 2D$ the $|\Delta\theta_{ext}|$ values are as high as 35°. Szepessy (1994) examined the phase drift of the vortex shedding signals versus the spanwise separation, where the phase drift was obtained according to the difference of zero-crossing time instants of the two signals measured at different spanwise locations. According to Szepessy (1994), the phase differences were about 32.60° and 50.40°, for $\Delta Z = D$ and $2D$, respectively, which are somewhat higher than our findings above.

Since the phase difference increases as the spanwise separation increases, it would reach 180° at some spanwise separation. Blevins (1985) and Szepessy & Bearman (1992) observed such situations, see table 2 for details. Unfortunately, the present study only provides data of the spanwise phase difference for $\Delta Z = D$ and $2D$.

In figures 10(*a*) and 10(*b*), the histograms are compared with the Gaussian distribution curves, indicated by the dashed lines. In the case of $\Delta Z = 2D$, figure 10(*b*)

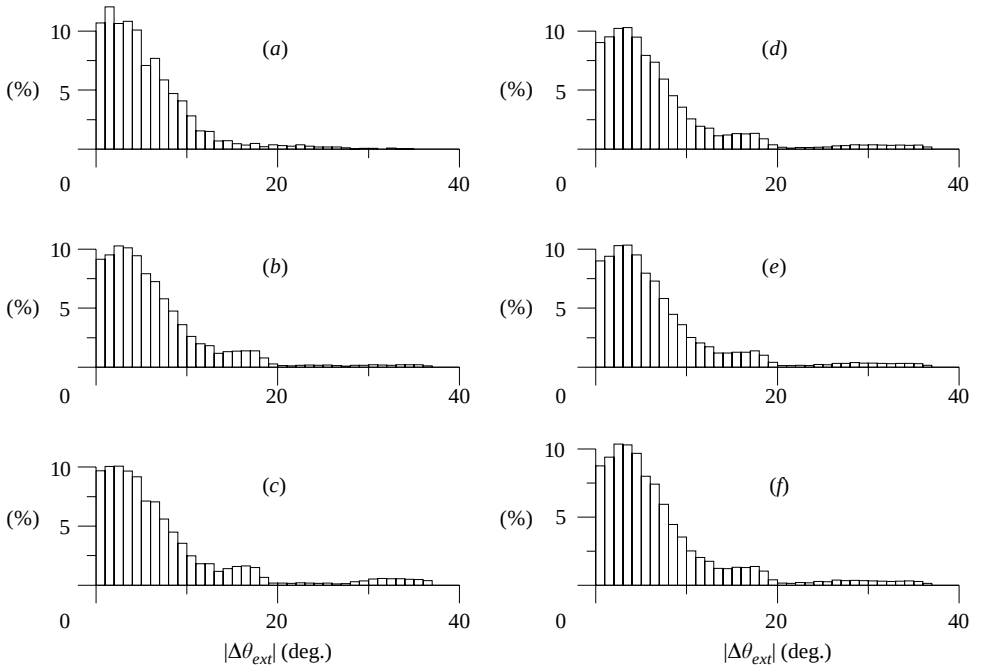

FIGURE 11. Histograms of $|\Delta\theta_{ext}|$ with S2 at $(X/D, Y/D, Z/D) = (1, 1.5, 0)$, for $\Delta Z = 2D$, at (*a*) $Re = 1800$, (*b*) $Re = 5200$, (*c*) $Re = 9800$, (*d*) $Re = 16\,000$, (*e*) $Re = 22\,500$, and (*f*) $Re = 27\,000$.

shows that the histogram distribution is in good agreement with the Gaussian distribution curve. This finding supports the statement made by Szepessy (1994), that the Gaussian distribution seems to fit well with the phase drift data when $\Delta Z/D = 2$ to 4. On the other hand, the histogram in figure 10(*a*) has a narrower distribution compared to the Gaussian curve.

Figure 10(*d*) indicates that the percentage of $|\Delta\theta_{ext}|$ between 20° and 35° is small but noticeable, signifying that these events deserve a further look. Further experiments were performed at lower Reynolds numbers, with the hot wire S2 at (X/D, Y/D, Z/D) = (1.0, 1.5, 0). Figure 11 presents the histograms of $|\Delta\theta_{ext}|$ obtained from these measurements, for $\Delta Z/D = 2$, showing that the events of $|\Delta\theta_{ext}|$ values in the range of 20° and 35° are indeed noticeable, despite the events of $|\Delta\theta_{ext}| < 5°$ occupying more than 50% of the total.

A Fourier analysis was made with the $\Delta\theta(t)$ data obtained. The spectral distributions, called $E(f_{\Delta\theta})$, are shown in figure 12. In each spectrum, the horizontal axis indicates the Fourier frequency, non-dimensionalized by the mean vortex shedding frequency, $f_{\Delta\theta}/f_s$. Figures 12(*a*) and 12(*b*) present the $E(f_{\Delta\theta})$ curves corresponding to $\Delta Z = D$ and $2D$, respectively, at all the Reynolds numbers studied. All the spectra shown in figure 12 reveal the common feature that the fluctuations in the frequency lower than $0.1 f_s$ are predominant, implying that the variations in the $\Delta\theta(t)$ curve are dominated by the frequency components one order smaller than f_s. This finding confirms the nature of low-frequency variations in the $\Delta\theta(t)$ curve.

4.5. *Cross-correlation between* $\Delta\theta(t)$ *and* $A_w(t)$

Figure 13 illustrates the cross-correlation analysis to examine the low-frequency variations embedded in $\Delta\theta(t)$ and $A_w(t)$. Figures 13(*a*) and 13(*b*) present the

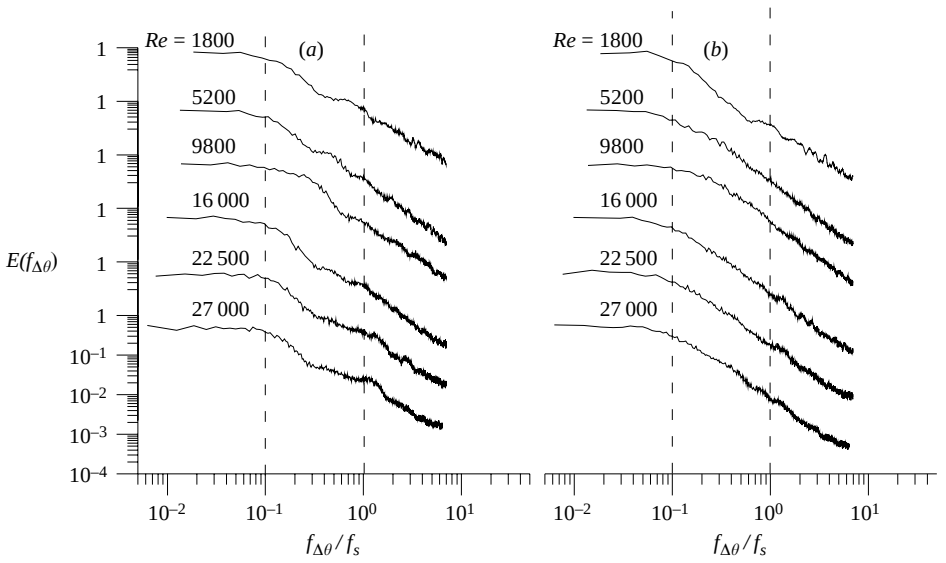

FIGURE 12. The frequency spectra of $\Delta\theta(t)$ obtained with S2 at $(X/D, Y/D, Z/D) = (1, 1.5, 0)$, for Re between 8×10^3 and 2.7×10^4, for (a) $\Delta Z = D$, (b) $\Delta Z = 2D$.

raw signals of hot wires S1 and S2, respectively, with hot wire S2 at $(X/D, Y/D, Z/D) = (1.0, 1.5, 0)$, for a time period equivalent to $240T_s$. The $f_w(t)$ curves of the hot-wire signals S1 and S2 are given in figure 13(c) for comparison. The corresponding $A_w(t)$ curves are given in figure 13(d), and the $\Delta\theta(t)$ curve is shown in figure 13(e).

In figures 13(d) and 13(e), the dashed line near $t/T_s = 100$ indicates the coinciding of a local minimum in $A_w(t)$ and a local maximum in $\Delta\theta(t)$, whereas the dotted line near $t/T_s = 160$ indicates another coinciding of a local minimum in $A_w(t)$ and a local minimum in $\Delta\theta(t)$. Similar coinciding can also be found at other time instants. These observations suggest that the correlation between the distinguished amplitude modulations and the notable phase differences, irrespective of whether they are positive or negative, could be meaningful.

The correlation coefficient between $A_w(t)$ for the signals S1 in figure 13(d), and $\Delta\theta(t)$ in figure 13(e) was found to be less than 0.3. On the other hand, the correlation coefficient of $A_w(t)$ and $|\Delta\theta(t)|$ in figure 13(f) was found to be -0.46, which appears to be much more significant. Figure 13(g) presents the results of a time-lag correlation between $A_w(t)$ and $|\Delta\theta(t+\tau)|$, where τ denotes the lag time in the correlation, ranging from $-120T_s$ to $120T_s$. The thick and thin curves in the figure indicate the correlation results of $|\Delta\theta(t+\tau)|$ with $A_w(t)$ of the hot-wire signals S1 and S2, respectively. Remarkably, the most significant correlation coefficients seen in the two curves occur at $\tau/T_s = 0$. This finding concurs with our intuitive thinking, that there would be no preferred phase lead or lag between $|\Delta\theta(t)|$ and $A_w(t)$, since the hot-wire signals were obtained at arbitrary spanwise points. As a counterpart of figure 13, figure 14(a) shows two $A_w(t)$ curves corresponding to the hot-wire signals S1 and S3, respectively; and figure 14(b) presents two $\Delta\theta(t)$ curves for S1–S2 and S1–S3, respectively. Figure 14(c) compares two time-lag correlation curves of $|\Delta\theta(t+\tau)|$ for S1–S2 and S1–S3, respectively, with $A_w(t)$ of the signal S1. Similar to figure 13(g), the two curves in figure 14(c) consistently show that the most significant correlation coefficients are

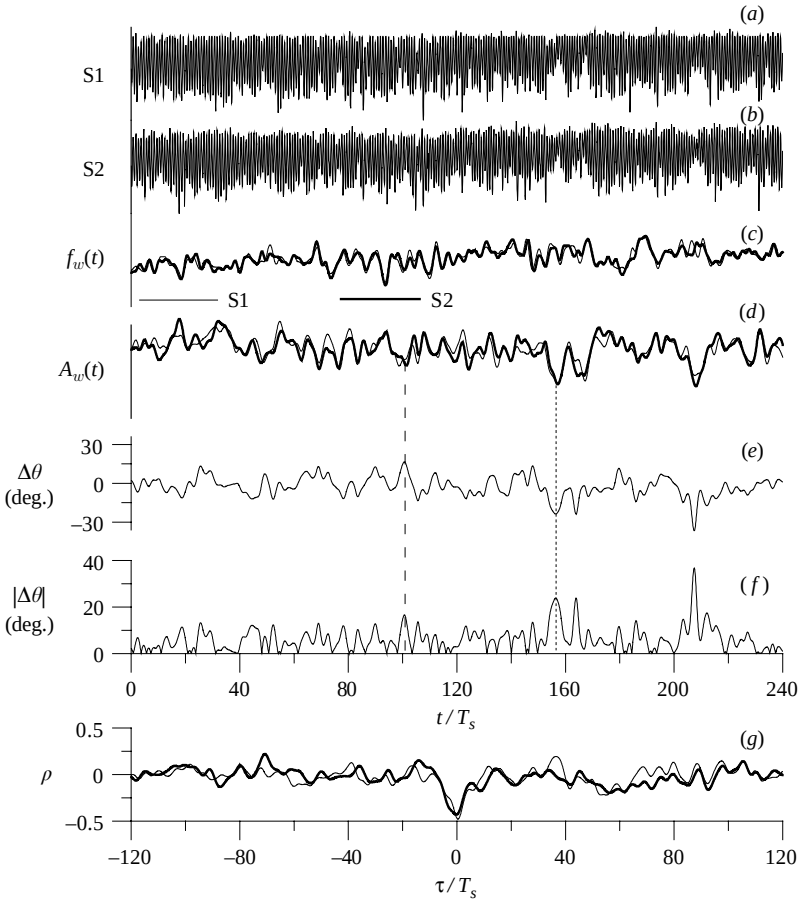

FIGURE 13. (*a*) Sampled hot-wire signals S1, at $Re = 27\,000$; (*b*) sampled hot-wire signals S2 obtained simultaneously, for S2 at $(X/D, Y/D, Z/D) = (1, 1.5, 0)$; (*c*) the $f_w(t)$ curves corresponding to the S1 and S2 signal traces; (*d*) the $A_w(t)$ curves corresponding to the S1 and S2 signal traces; (*e*) the $\Delta\theta(t)$ curve reduced from (*c*); (*f*) the $|\Delta\theta|$ curve obtained from (*e*); (*g*) the time-lag correlation coefficients between $|\Delta\theta|$ and $A_w(t)$ of the S1 and S2 signal traces.

obtained at $\tau/T_s = 0$. The correlation coefficient between $|\Delta\theta(t+\tau)|$ of S1–S3 and $A_w(t)$ of S1 at $\tau/T_s = 0$ is found to be -0.43.

It is noted in figures 13 and 14 that the correlation coefficients of $|\Delta\theta(t+\tau)|$ and $A_w(t)$ at $\tau/T_s = 0$ do not vary much between $\Delta Z = D$ and $2D$. Further confirmation of this observation is seen in figure 15, in which the zero time-lag correlation coefficients between $A_w(t)$ and $|\Delta\theta(t)|$ at all the Reynolds numbers studied, for $\Delta Z = D$ and $2D$, are presented. The measurements were made with the hot wire S2 located at $(X/D,\ Y/D,\ Z/D) = (1.0,\ 1.5,\ 0)$. In this figure, each of the data points indicates the value obtained by averaging over 30 sets of data, and an I-bar indicates the associated 95% confidence interval. Since the $A_w(t)$ and $\Delta\theta(t)$ curves feature low-frequency modulations, this figure strongly suggests that the low-frequency modulations correlate well in the range of Reynolds numbers studied, irrespective of whether $\Delta Z = D$ or $2D$. Norberg (2003) compiled results from quite a number of experimental studies on spanwise vortex shedding for flows over a circular cylinder, and found that the spanwise correlation length of shedding vortices ranges from $3D$

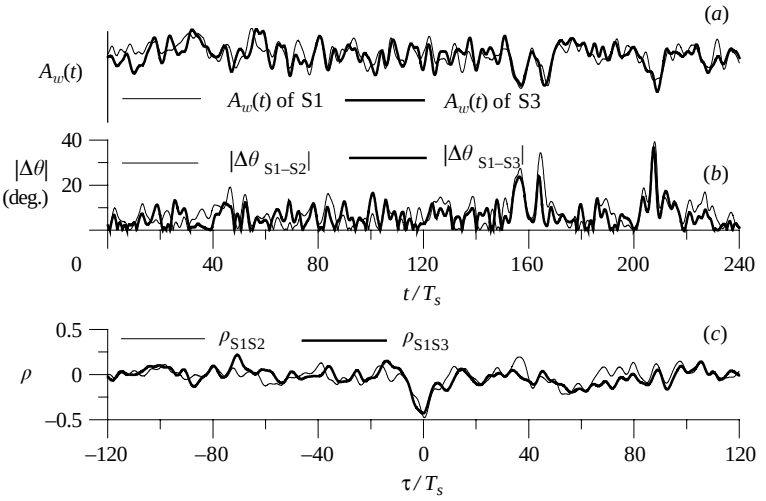

FIGURE 14. (*a*) The $A_w(t)$ curves obtained from the S1 and S3 signal traces, at $Re = 27\,000$; (*b*) the $|\Delta\theta|$ curves of S1–S2, and S1–S3, (*c*) the time-lag correlation distributions between $|\Delta\theta|$ of S1–S2 and $A_w(t)$ of the S1 signal trace, and between $|\Delta\theta|$ of S1–S3 and $A_w(t)$ of the S1 signal trace. S2 was at $(X/D, Y/D, Z/D) = (1, 1.5, 0)$.

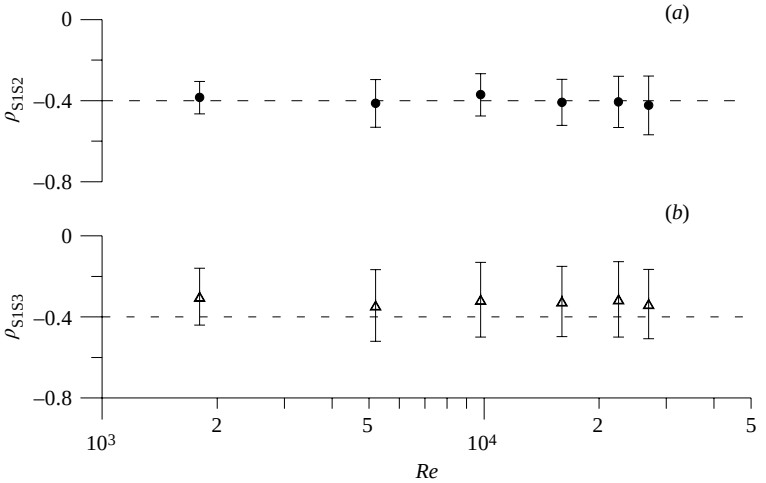

FIGURE 15. The zero time-lag correlation coefficients between $A_w(t)$ of the S1 signal trace and: (*a*) $|\Delta\theta|$ of S1–S2 and (*b*) $|\Delta\theta|$ of S1–S3, at $Re = 1800$ to 27 000. S2 was at $(X/D, Y/D, Z/D) = (1, 1.5, 0)$.

to $8D$ at Reynolds numbers of 10^3 to 10^4. The results presented in figure 15 are specifically concerned with the low-frequency modulations embedded in the vortex shedding signals.

A close look at the curves in figures 13(*c–e*) immediately shows that large $\Delta\theta$ values frequently occur when discrepancies between the $f_w(t)$ curves of S1 and S2 are discernible, for instance at the time around $t/T_s = 210$. Referring to Williamson (1992), Yang *et al.* (1993), and Braza, Faghani & Persillon (2001), the significant differences between the shedding frequencies measured at different spanwise locations can be associated with the passage of vortex dislocation. In figures 13(*a*) and 13(*b*),

both hot-wire signals S1 and S2 show weak shedding cycles around $t/T_s = 210$, for which the fluctuating amplitudes, $A_w(t)$, appear to be at low values. Norberg (2003) conjectured that the occurrence of vortex dislocation is associated with weak shedding periods. Henderson (1997) pointed out that the localized phase dislocations of vortex shedding were responsible for modulating the amplitude of fluctuating lift and drag, based on numerical results at Reynolds number 1000. Based on the present findings and the observations above, one can further argue that vortex dislocation, weak vortex shedding, and large spanwise phase difference probably occur concurrently in the process of vortex shedding.

Following the argument above, it is seen in figure 13(*c*) that the vortex shedding frequencies of the hot-wire signals S1 and S2 appear to stay very close to each other most of time, except during the time intervals when the $A_w(t)$ values are low, when the discrepancies are notable. These local appearances could imply the occurrences of vortex dislocation. Moreover, these time intervals frequently coincide with the occurrence of large inclination angle $\Delta\theta$ seen in figure 13(*e*), and thus are very likely associated with the development of the spanwise cells seen in figure 3. Hence, one can say that figures 13 and 14 explain well the occurrence of unsteady, spanwise cellular structures in the near-wake region addressed in Szepessy & Bearman (1992).

In summary, figures 13, 14 and 15 clarify that the three-dimensionality in shedding vortices is quite pronounced when the amplitude $A_w(t)$ appears to be small, at which the spanwise phase difference of vortex shedding appears to be rather large. This explains why the correlation coefficient of $|\Delta\theta(t)|$ and $A_w(t)$ is negative. Figure 15 shows that all the correlation coefficients obtained are about -0.4, irrespective of whether $\Delta Z = D$ or $2D$.

4.6. *Unsteady, three-dimensional characteristics of flow in the near-wake region*

Referring to figures 16(*a*) and 16(*b*), two distinct situations concerning vortex formation in the near-wake region will be discussed in this section. In the figures, sketches are provided to assist in explanation. In each of the sketches, the thick solid line, indicating the smoke streak pattern in the corresponding photograph, is intended to highlight the extent of the vortex formation region; the dashed line indicates the streamwise extent of the vortex formation region, in a hypothetical situation, that would be uniform along the span. However, given the fact that a shedding vortex in the near-wake region can easily develop a three-dimensional appearance, one should keep in mind that the sketches and the photographs in figure 16 can only represent very limited aspects of vortex formation.

Comparing the photographs in figures 16(*a*) and 16(*b*), one immediately sees that the vortex formation length varies widely in streamwise extent. In figure 16(*a*), the vortex formation length is comparatively long, and the vortex formation region appears to be rather uniform along the span. On the other hand, in figure 16(*b*), the vortex formation length is comparatively short, and its streamwise extent region appears to be very irregular along the span. The characteristics associated with the two distinct vortex shedding situations, highlighted in figures 16(*a*) and 16(*b*), are further described below.

(i) Long formation region mode, called Mode L: As illustrated in figure 16(*a*), the formation length is normally larger than $2D$. From Miau *et al.* (1999, 2003), the base pressure measured in this situation is comparatively high. Moreover, figure 13(*c*) shows that the vortex shedding frequency obtained in this situation is comparatively low, whereas the fluctuating amplitude of the vortex shedding signals, $A(t)$, appears to be rather high and the spanwise phase difference, $\Delta\theta(t)$, is low.

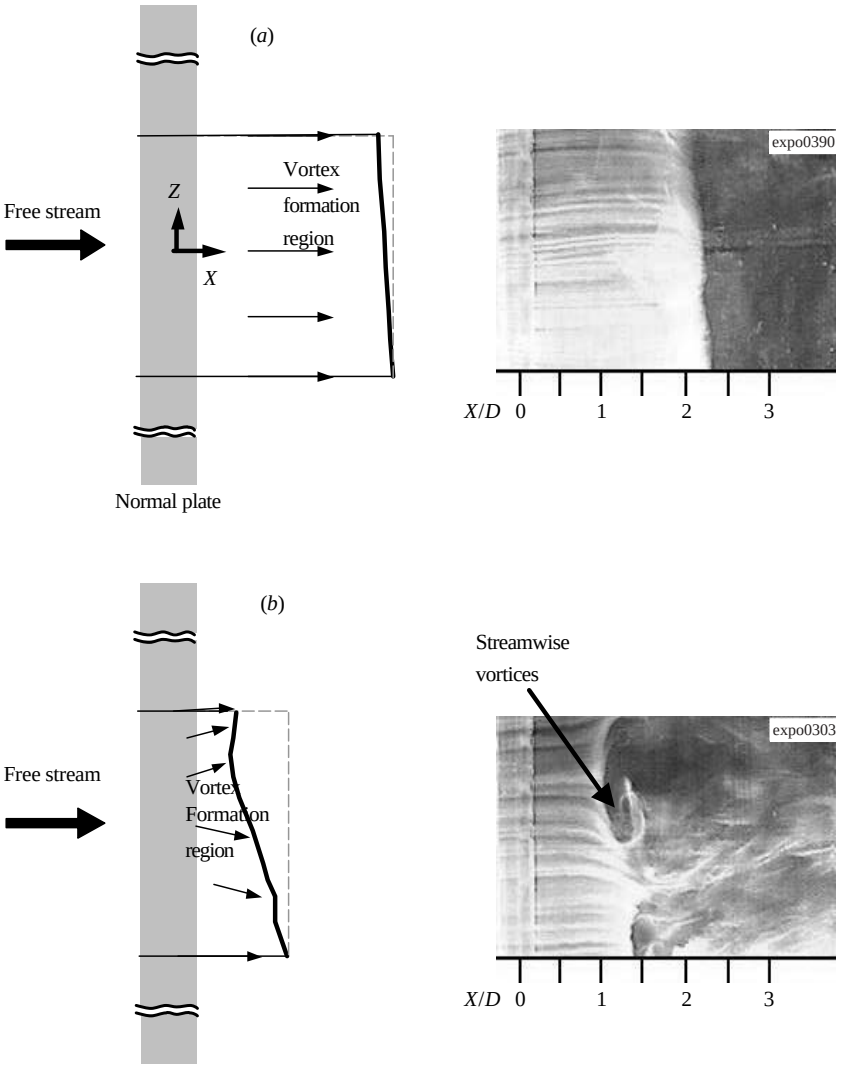

FIGURE 16. Illustrations of two extreme modes of vortex formation. (*a*) Mode L: long formation region mode; (*b*) Mode S: short formation region mode.

(ii) Short formation region mode, called Mode S: As illustrated in figure 16(*b*), the formation length is definitely shorter than $2D$. Accordingly, the base pressure measured would be considerably lower, and the vortex shedding frequency comparatively higher than for Mode L, whereas the corresponding $A(t)$ and $\Delta\theta(t)$ values are lower and higher, respectively.

From the descriptions above, the events of large $|\Delta\theta_{ext}|$ values in figures 10 and 11 are likely to be described as Mode S. Also, the flow images in the photographs in figure 3(*b*) can be described as Mode S, could be the vortex formation length shown can be as short as D. Clearly, as Mode S appears to be less stable, because of the lower base pressure (Miau *et al.* 2003), the short vortex formation region, is apt to develop a three-dimensional appearance. On the other hand, referring to Bearman (1997), the longer vortex formation length in Mode L gives the opportunity for more

vorticity mixing and cancellation, and hence the condition of near constant circulation flux across the span is possible.

Najjar & Balachandar (1998) performed a numerical study, and found that the vortex formation length varies with time at a fixed Reynolds number, 250. They also pointed out that the three-dimensionality of the wake behind a normal plate behaves in two distinct modes, namely a regime H corresponding to high mean drag and a regime L corresponding to low mean drag. In regime H, the shear layer rolls up closer to the plate to form coherent spanwise vortices and organized streamwise vortices. In regime L, the spanwise vortices form farther from the base, and are less coherent while the streamwise vortices are spatially distributed. The similarity between the findings of Najjar & Balachandar (1998) and the present study deserves some discussion here. The regime H of high mean drag looks similar to Mode S here, in that organized streamwise vortices are noted in both studies. On the other hand, there are some discrepancies between regime L of Najjar & Balachandar (1998) and Mode L here. According to the present flow visualization, in Mode L, the streamwise vortices are less pronounced and the shedding vortices appear to be quite coherent along the span. It should also be pointed out that the Reynolds number in Najjar & Balachandar's (1998) study, 250, is considerably lower than the present ones. Referring to Zdravkovich (1996), the Reynolds number of Najjar & Balachandar (1998) falls in the transition-in-wake (TrW) state, whereas the Reynolds numbers of the present study are in the transition-in-shear-layers ($TrSL$) state. According to Zdravkovich (1996), the differences between the mechanisms of eddy shedding of TrW and $TrSL$ states are that the former is related to the laminar wake instability and the latter to full growth and shedding of eddies. Unfortunately, no numerical results relevant to the Reynolds numbers in the $TrSL$ state appear to be available in the literature.

From the standpoint of three-dimensional flow instabilities, Williamson (1996) stated that the natural wake transition follows the sequence (2-D→mode A→mode B) in the range of Reynolds numbers from less than 160 to 230. Briefly, mode A instability is associated with the inception of streamwise vortex loops, and mode B instability is associated with the finer-scale streamwise vortex pairs. Lin, Towfighi & Rockwell (1995) suggested a predominant role of a convective instability (Huerre & Monkewitz 1985) leading to large-scale vortex formation at $Re = 10^3$, as opposed to a global instability (Barkley & Henderson 1996) of the near wake that gives rise to large-amplitude, self-sustained oscillations in the very near wake region as the Reynolds number increases to 10^4. However, Norberg (2003) suggested that, up to $Re = 5 \times 10^3$, the transition to turbulence has its origin in the near-wake development of rib-like mode B vortices. To sum up, there could be a number of flow instability mechanisms coexisting in the present range of Reynolds numbers, leading to the three-dimensionality and low-frequency modulations in vortex shedding. Even when the Reynolds number is fixed, the effects of these instabilities would vary temporally to some degree, as revealed by the instantaneous flow behaviours reported in the forgoing sections. Further comments on the temporal characteristic of Modes L and S will be made in the following.

4.7. *Burst events in the vortex shedding process*

The histograms in figure 11 show that the probability associated with the events of $\Delta\theta_{ext}$ larger than 20° is noticeable, although small. Moreover, the flow visualization photographs in figure 3(*b*) show that the events of Mode S are probably involved with the development of the secondary vortices. In this section, physical aspects of these events will be further discussed.

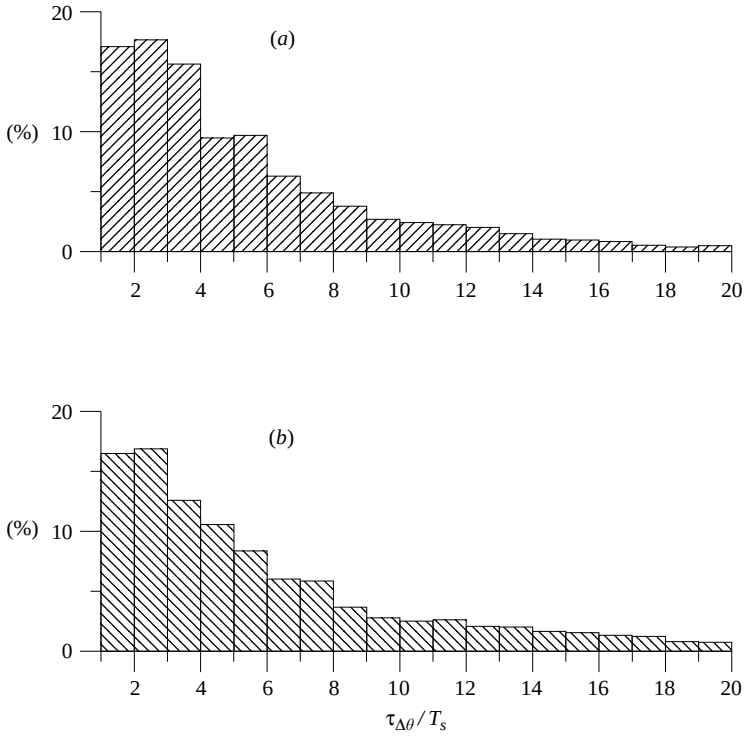

FIGURE 17. Histograms of $\tau_{\Delta\theta}/T_s$, for $Re = 27\,000$, for (*a*) $\Delta Z = D$, (*b*) $\Delta Z = 2D$. S2 was at $(X/D, Y/D, Z/D) = (1, 1.5, 0)$.

Statistically speaking, these events occupy only about 5% of the time. However, they are accompanied by strong development of secondary vortices, which conceivably is involved with the mechanism of vorticity stretching, leading to strong momentum mixing in a three-dimensional fashion. Hence, the events are called burst events here. One can argue that these events play the role of reducing the spanwise phase difference of vortex shedding to minimum, thus the vortex shedding process becomes Mode L.

In considering this moderating process, a quantity denoted $\tau_{\Delta\theta}$, the time interval between two neighbouring zero-crossing points on a $\Delta\theta$ curve, is proposed to characterize a cycle of the variations of the vortex formation length. Two histograms of $\tau_{\Delta\theta}$, normalized by T_s, obtained at $Re = 27\,000$, for $\Delta Z = D$ and $2D$, respectively, are shown in figure 17. Note that the $\Delta\theta(t)$ data employed for analysis are identical to those in figure 10. Because events of $\tau_{\Delta\theta}/T_s > 20$ occupy less than 0.4% of the total, they are ignored. The probability in the range within $10 < \tau_{\Delta\theta}/T_s < 20$ is noticeable, despite the major portion of the events falling in the region of $\tau_{\Delta\theta}/T_s < 10$. In order to learn more about the characteristics of $\tau_{\Delta\theta}/T_s$, figure 18 presents a distribution of $\Delta\theta_{ext}$ versus $\tau_{\Delta\theta}/T_s$. Although the data points in figure 18 appear to somewhat scattered, it is easy to recognize the trend that the data points follow a positive slop, which can be fitted by the linear curve shown. Namely, the larger the spanwise phase difference of vortex shedding, the more time is needed to recover to in-phase shedding. The dashed line indicating $\Delta\theta_{ext} = 20^\circ$ in the figure divides the data points into two regions. The histograms in figures 10 and 11 show that $\Delta\theta_{ext} = 20^\circ$ seems to be a

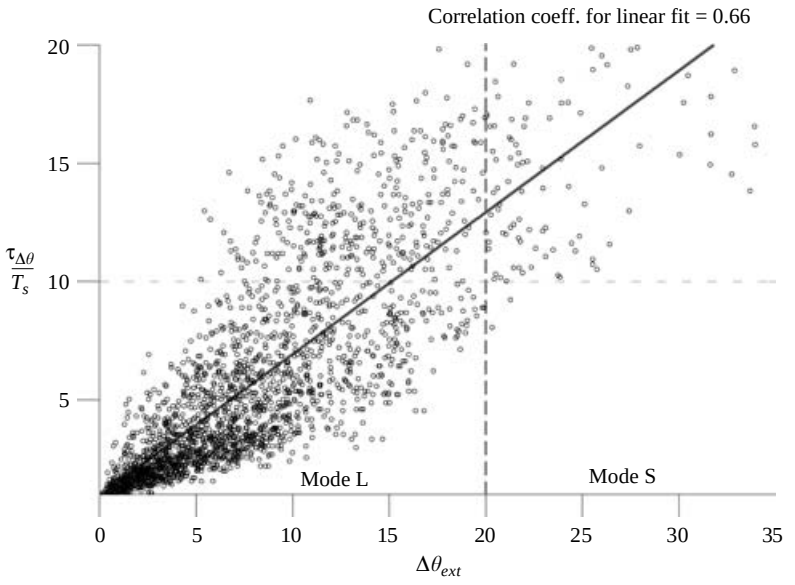

FIGURE 18. Distribution of $\Delta\theta_{ext}$ versus $\tau_{\Delta\theta}/T_s$, for $\Delta Z = D$, at $Re = 27\,000$. S2 was at $(X/D, Y/D, Z/D) = (1, 1.5, 0)$.

good choice to differentiate two regions of small and large values of $\Delta\theta_{ext}$, namely, the situations of Modes L and S, respectively.

Figure 18 suggests that the $\tau_{\Delta\theta}$ values in Mode S fall in the range $10T_s$ to $20T_s$. At the same time, Szepessy (1994) found that the time scale corresponding to the pronounced oscillations in the short-time correlation between two signals obtained for $\Delta Z = D$ and $2D$ are 10 to 20 times the vortex shedding periods. The abrupt, steep drops in the short-time correlation trace described by Szepessy (1994) very likely correspond to the burst events of Mode S mentioned above.

In summary, the burst events of Mode S feature large spanwise phase differences in vortex shedding. The events are involved with the development of secondary vortices promoting momentum mixing, and lead to a moderation of spanwise phase difference to produce Mode L. The duration of this process is $10T_s$ to $20T_s$. It should be noted that the development of the secondary vortices clearly causes the three-dimensional distortion of shedding vortices, thus the effects of vorticity tilting and stretching should come into play in the dynamical process; this is not pursued further in this study.

In their numerical studies, Najjar & Balachandar (1998) pointed out that the low-frequency unsteadiness appears to be asymmetric, resulting in a relatively longer duration of low-mean drag, separated by comparatively shorter duration of intense vortex shedding and high mean drag. The duration of high mean drag is similar to Mode S described above, although the Reynolds numbers of these two studies are very different. The numerical results of Henderson (1997) at a Reynolds number of 10^3 showed that the dislocation of vortical structures appears intermittently in time and randomly in the spanwise direction. Unfortunately, Najjar & Balachandar (1998) and Henderson (1997) did not provide quantitative information on the time duration of these strongly three-dimensional events.

The term 'burst' is used in a number of reports on the vortex shedding phenomenon as summarized in table 3 for reference. The definitions of burst in these reports are

Source	Re ($\times 10^3$)	Method of study	Location in the flow field	Findings associated with burst	Physical descriptions concerning bursts and three-dimensionality
Bloor (1964)	5.2	Hot wire	In the wake region	Transition waves appeared in velocity signals	Transition develops as 2D instability, through small-scale three-dimensionalities to turbulence
Toebes (1969)	68	Hot wires	$Y/D = 0.56 \sim 0.8$	Sudden changes in amplitude, i.e. spikes, in velocity signals	
Blevins (1985)	40	Flush film; microphone	Surface, 90°	Large amplitudes in the velocity and pressure signal traces	The bursts seen in all the sensor signals along the span suggest a quasi-2D vortex shedding structure
Norberg (1989)	36	Hot wire; microphone	$X/D = 0$, $Y/D = 0.6$	Large amplitudes in the velocity and pressure signals	The bursts are probably related to the 3D evolution of vortices
Szepessy & Bearman(1992)	$8 \sim 140$	Hot wire; pressure tap	$X/D = 0$, $Y/D = 0.8$	Irregularity in vortex shedding strength shown by the velocity and pressure signals	The burst-like appearance is the main 3D feature of vortex shedding
Roshko (1993) Lisoski (1993)	$1 \sim 15$	Force balance		Lift and drag measurements appear in bursts	Associated with the spanwise modulation of vortex shedding phase
Henderson (1997)	1	Numerical		Lift and drag measurements appear in burst at irregular intervals	Associated with vortex dislocation
Present study	$1.8 \sim 27$	Hot wire	Outside the separated shear layer	Spanwise phase difference of vortex shedding larger than 20°	The three-dimensionality is most pronounced in the burst events

TABLE 3. A survey on the term 'burst' appearing in studies on the vortex shedding process.

not identical to the present study. Roshko (1993) quoted the experimental lift and drag histories of a bluff plate at Reynolds number 6×10^3 measured by Lisoski (1993), and remarked that the fluctuations of lift and drag appear in bursts, which bear a similarity to the results of Henderson (1997). Blevins (1985) and Norberg (1989) referred to events of large amplitude in the vortex shedding signals as bursts. Bloor (1964) related bursts to transition waves detected. In the present study, the burst events refer to situations when Mode S takes place, for which the vortex formation length appears to be short, and the development of a separated shear layer is strongly involved with secondary vortices. This process is named a burst is because of its infrequent occurrence in vortex shedding, occupying only about 5% of the total time; when it does occur, strong three-dimensional mixing associated with the secondary vortices is anticipated. Clearly, these events are an important feature of the unsteady, three-dimensional flow in the near-wake region.

5. Conclusions

The experimental efforts reported above were aimed at gaining a better understanding of the instantaneous behaviour of the unsteady, three-dimensional flow in the near-wake region. Velocity measurements obtained simultaneously at three spanwise points allowed the linkage between the spanwise phase differences of shedding vortices and low-frequency modulations embedded in the vortex shedding signals to be examined. An important finding is that the vortex shedding process consists of a string of burst events occuring sporadically in time, during which the three-dimensionality of shedding vortex appears to be very pronounced, involved with strong development of secondary vortices. When these events take place, the vortex formation length is significantly reduced, referred to as Mode S. Apart from the occurrence of these events, the vortex shedding process features a longer vortex formation length, referred to as Mode L, for which the three-dimensional appearance of shedding vortices is less pronounced.

The specific findings relevant to these flow characteristic are summarized below.

(i) The events of $|\Delta\theta_{ext}|$ larger than 20°, referred to as Mode S, occur in less than 5% of the total time measured. These events are termed 'burst' events in the vortex shedding process. The time scale associated with the burst events is $10T_s$ to $20T_s$, comparable to the characteristic time scale of low-frequency modulations seen in the vortex shedding signals measured.

(ii) The cross-correlation between the spanwise phase difference, $|\Delta\theta(t)|$, and the fluctuating amplitude of the instantaneous vortex shedding frequency, $A_w(t)$, is very significant, irrespective of whether $\Delta Z = D$ or $2D$. The correlation coefficients obtained are about -0.4. This finding confirms that when $|\Delta\theta(t)|$ is large, i.e. in the situation of Mode S, $A_w(t)$is likely to be small. Such an event is referred to as weak shedding in the literature, and is probably associated with the development of vortex dislocation.

(iii) The $|\Delta\theta(t)|$ histograms show that most of the values fall in the range of 0 to 35°, irrespective of whether $\Delta Z = D$ or $2D$ and the Reynolds numbers studied. The $|\Delta\theta(t)|$ histograms of $\Delta Z = 2D$ appear to be similar to a Gaussian distribution; on the other hand, the $|\Delta\theta(t)|$ histograms of $\Delta Z = D$ show a narrower distribution.

(iv) The spectral distributions of $\Delta\theta(t)$ show a sharp decrease as the frequency becomes larger than $0.1f_s$, which is the same as the characteristic behaviour of low-frequency modulations in the vortex shedding signals.

The present efforts have lead to an important finding concerning the events of Mode S in the vortex shedding process. However, the dynamical aspects of these events are not well-understood yet. For instance, the burst events, which are involved with the development of secondary vortices, require further study to explore the effects of vorticity stretching and tilting. The transition process between the Modes L and S, which was not considered in the present study, deserves a careful look.

To gain further insight into the instantaneous, three-dimensional behaviour of this wake flow, one might consider employing other relevant measurement techniques, for instance the PIV technique, which would enable one to obtain quantitative information on the vortex formation length in the instantaneous sense. To study the inception of the three-dimensionality of the separated shear layer, one might consider employing some miniature sensors suitable for probing the flow characteristics in the vicinity of the sharp edge of the normal plate.

The authors would like to acknowledge the support of National Science Council, Taiwan, for this work, with the contract number of NSC 91-2212-E-006-046.

REFERENCES

Barkley, D. & Henderson, R. 1996 Three-dimensional floquet stability analysis of the wake of a circular cylinder. *J. Fluid Mech.* **322**, 215–241.

Bays-Muchmore, B. & Ahmed, A. 1993 Three-dimensional shear layers via vortex dynamics. *J. Fluid Mech.* **189**, 87–116.

Bearman, P. W. 1997 Near wake flows behind two- and three-dimensional bluff bodies. *J. Wind Engng Indust. Aerodyn.* **69**, 33–54.

Bearman, P. W. & Tombazis, N. 1993 The effects of three-dimensional imposed disturbances on bluff body near wake flows. *J. Wind Engng Indust. Aerodyn.* **49**, 339–350.

Bendat, J. S. & Piersol, A. G. 1991 *Random Data Analysis and Measurement Procedure*, 2nd edn. John Wiley & Sons.

Berger, E., Scholz, D. & Schumm, M. 1990 Coherent vortex structures in the wake of a sphere and a circular disk at rest and under force vibrations. *J. Fluids Struct.* **4**, 231–257.

Blackburn, H. M. & Melbourn, W. H. 1996 The effect of free-stream turbulence on sectional lift forces on a circular cylinder. *J. Fluid Mech.* **306**, 267–292.

Blevins, R. D. 1985 The effect of sound on vortex shedding from cylinders. *J. Fluid Mech.* **161**, 217–237.

Bloor, M. S. 1964 The transition to turbulence in the wake of a circular cylinder. *J. Fluid Mech.* **19**, 290–304.

Bloor, M. S. & Gerrard, J. H. 1966 Measurements on turbulent vortices in a cylinder wake. *Proc. R. Soc. Lond.* A **294**, 319–342.

Braza, M., Faghani, D. & Persillon, H. 2001 Successive stages and the role of natural vortex dislocations in three-dimensional wake transition. *J. Fluid Mech.* **439**, 1–41.

Carmona, R. A., Hwang, W. L. & Torrésani, B. 1997 Characterization of signals by the ridges of their wavelet transform. *IEEE Trans. Signal Process.* **45**, 2586–2590.

Cimbala, J. M., Nagib, H. M. & Roshko, A. 1988 Large structure in the far wakes of two-dimensional bluff bodies. *J. Fluid Mech.* **190**, 265–298.

Davies, M. E. 1976 A comparison of the wake structure of a stationary and oscillating bluff body, using a conditional averaging technique. *J. Fluid Mech.* **75**, 209–231.

Farge, M. 1992 Wavelet transforms and their applications to turbulence. *Annu. Rev. Fluid Mech.* **24**, 395–457.

Fox, T. A. & West, G. S. 1990 On the use of end plates with circular cylinders. *Exps. Fluids* **9**, 231–239.

Gaster, M. 1969 Vortex shedding from slender cones at low Reynolds numbers. *J. Fluid Mech.* **38**, 565–576.

Gerich, D. & Eckelmann, H. 1982 Influence of end plates and free ends on the shedding frequency of circular cylinders. *J. Fluid Mech.* **122**, 109–121.

Gerrard, J. H. 1966 The three-dimensional structure of the wake of a circular cylinder. *J. Fluid Mech.* **25**, 143–164.

Gerrard, J. H. 1967 Experimental investigation of separated boundary layer undergoing transition to turbulence. *Phys. Fluids* **10**, S98–S100.

Graham, J. M. R. 1969 The effect of end-plates on two-dimensionality of a vortex wake. *Aeronaut. Q.* **20**, 237–247.

Grant, H. L. 1958 The large eddies of turbulent motion. *J. Fluid Mech.* **4**, 149–190.

Grossman, A. & Morlet, J. 1984 Decomposition of Hardy functions into square integrable wavelets of constant shape. *SIAM J. Math. Anal.* **15**, 723–736.

Hamdan, N. N., Jurban, B. A., Shabaneh, N. H. & Abu-Samak, M. 1996 Comparison of various basic wavelets for the analysis of flow-induced vibration of a cylinder in cross flow. *J. Fluids Struct.* **10**, 633–651.

Hanson, F. B. & Richardson, P. D. 1968 The near-wake of a circular cylinder in cross flow. *Trans. ASME: J. Basic Engng* **90**, 476–484.

Henderson, R. C. 1997 Nonlinear dynamics and pattern formation in turbulent wake transition. *J. Fluid Mech.* **352**, 65–112.

Huerre, P & Monkewitz, P. A. 1985 Absolute and convective instabilities in free shear layers. *J. Fluid Mech.* **159**, 151–168.

Humphreys. J. S. 1960 On a circular cylinder in a steady wind at transition Reynolds numbers. *J. Fluid Mech.* **9**, 603–612.

Ishikawa, H., Kiya, M., Komaki, Y. & Mochizuki, O. 1996 Low-frequency modulation of turbulent Karman vortex street. *Trans. JSME* B **62**, 2180–2186.

Kiya, M. & Abe, Y. 1999 Turbulent elliptic wakes. *J. Fluids Struct.* **13**, 1041–1067.

Lewis, C. G. & Gharib, M. 1992 An exploration of the wake three dimensionalities caused by a local discontinuity in cylinder diameter. *Phys. Fluids* A **4**, 104–117.

Lin, J.-C., Towfighi, J. & Rockwell, D. 1995 Instantaneous structure of the near-wake of a circular cylinder: on the effect of Reynolds number. *J. Fluids Struct.* **9**, 409–418.

Lisoski, D. 1993 Nominally 2-dimensional flow about a normal flat plate. PhD thesis, California Institute of Technology.

Mansy, H., Yang, P.-M. & Williams, D. R. 1994 Quantitative measurements of three-dimensional structures in the wake of a circular cylinder. *J. Fluid Mech.* **270**, 277–296.

Miau, J. J., Wang, J. T., Chou, J. H. & Wei, C. Y. 1999 Characteristics of low-frequency variations embedded in vortex shedding process. *J. Fluids Struct.* **13**, 339–359.

Miau, J. J., Wang, J. T., Chou, J. H. & Wei, C. Y. 2003 Low-frequency fluctuations in the near wake region of a trapezoidal cylinder with low aspect ratio. *J. Fluids Struct.* **17**, 701–715.

Miau, J. J., Wu, S. J., Hu, C. C. & Chou, J. H. 2004 Low-frequency modulations associated with vortex shedding due to flow over a bluff body. *AIAA J.* **42,** 1388–1397.

Miau, J. J., Yang, C. C., Chou, J. H. & Lee, K. R. 1993 Suppression of low-frequency variations in vortex shedding by a splitter plate behind a bluff body. *J. Fluids Struct.* **7**, 897–912.

Najjar, F. M. & Balachandar, S. 1998 Low- frequency unsteadiness in the wake of a normal flat plate. *J. Fluid Mech.* **370**, 101–147.

Noack, B. R., König, M. & Eckelmann, H. 1993 Three-dimensional stability analysis of the periodic flow around a circular cylinder. *Phys. Fluids* A **5**, 1279–1281.

Norberg, C. 1989 An experimental study of the circular cylinder in cross flow: transition around $Re = 5 \times 10^3$. 4th *Asian Cong. Fluid Mech. Hong Kong* (ed. W. M. Ko & S. C. Kot), C240–243. The University of Hong Kong.

Norberg, C. 1994 An experimental investigation of the flow around a circular cylinder: influence of aspect ratio. *J. Fluid Mech.* **258**, 287–316.

Norberg, C. 2003 Fluctuating lift on a circular cylinder: review and new measurements. *J. Fluid Struct.* **17**, 57–96.

Roshko, A. 1954 On the development of turbulent wakes from vortex streets. *NACA Rep.* 1191.

Roshko, A. 1993 Perspectives on bluff body aerodynamics. *J. Wind Engng Indust. Aerodyn.* **49**, 79–100.

Stäger, R. & Eckelmann, H. 1991 The effect of endplates on the shedding frequency of a circular cylinders in the irregular range. *Phys. Fluids* A **3**, 2116–2121.

Stansby, P. K. 1974 The effects of end plates on the base pressure coefficients of a circular cylinder. *Aeronaut. J.* **78**, 36–37.

Szepessy, S. 1994 On the spanwise correlation of vortex shedding from a circular cylinder at high subcritical Reynolds number. *Phys. Fluids* A **6**, 2406–2416.

Szepessy, S. & Bearman P. W. 1992 Aspect ratio and end plate effects on vortex shedding from a circular cylinder. *J. Fluid Mech.* **234**, 191–217.

Taneda, S. 1978 Visual observations of the flow past a sphere at Reynolds numbers between 104 and 106. *J. Fluid Mech.* **85**, 187–192.

Toebes, G. H. 1969 The unsteady flow and wake near an oscillating cylinder. *Trans. ASME: J. Basic Engng* **91**, 493–505.

Torrence, C. & Compo, G. P. 1998 A practical guide to wavelet analysis. *Bull. Am. Met. Soc.* **79**, 61–78.

Tritton, D. J. 1959 Experiments on the flow past a circular cylinder at low Reynolds number. *J. Fluid Mech.* **16**, 547–567.

Van Atta, C. W. & Gharib, M. 1987 Ordered and chaotic vortex streets behind circular cylinders at low Reynolds numbers. *J. Fluid Mech.* **174**, 113–133.

Wang, C. T. 2000 Investigation of low frequency variations embedded in vortex shedding process. PhD thesis, National Cheng Kung University, Taiwan.

Wei, T. & Smith, C. R. 1986 Secondary vortices in the wake of circular cylinder. *J. Fluid Mech.* **169**, 513–553.

Williamson, C. H. K. 1988 The existence of two stages in the transition to three dimensionality of a cylinder wake. *Phys. Fluids* **31**, 3165–3167.

Williamson, C. H. K. 1992 The natural and forced formation of spot-like vortex dislocations in the transition of a wake. *J. Fluid Mech.* **243**, 393–441.

Williamson, C. H. K. 1996 Vortex dynamics in the cylinder wake. *Annu. Rev. Fluid Mech.* **28**, 477–539.

Wu, J., Sheridan, J., Soria, J. & Welsh, M. C. 1994 An experimental investigation of streamwise vortices in the wake of a bluff body. *J. Fluids Struct.* **8**, 621–625.

Wu, S. J. 2003 Instantaneous properties of low-frequency modulations and three-dimensionality associated with vortex shedding. PhD thesis, National Cheng Kung University, Tainan, Taiwan.

Yang, P.-M., Mansy, H. & Williams, D. R. 1993 Oblique and parallel wave interaction in the near-wake of a circular cylinder. *Phys. Fluids* A **5**, 1657–1661.

Zdravkovich, M. M. 1996 *Flow around Circular Cylinders*, vol. 1. Oxford University Press.